ALPACA - A kinetic theory Monte Carlo event generator for heavy ion collisions

Törnkvist, Robin

2023

ALPACA - A kinetic theory Monte Carlo event generator for heavy ion collisions

ROBIN TÖRNKVIST
DEPARTMENT OF PHYSICS | FACULTY OF SCIENCE | LUND UNIVERSITY

Printed by Media-Tryck, Lund 2023 NORDIC SWAN ECOLABEL 3041 0903

Faculty of Science
Department of Physics

ISBN 978-91-8039-817-6

ALPACA - A kinetic theory Monte Carlo event generator for heavy ion collisions

ALPACA - A kinetic theory Monte Carlo event generator for heavy ion collisions

by Robin Törnkvist

LUND
UNIVERSITY

Thesis for the degree of Doctor of Philosophy
Thesis advisor: Korinna Zapp
Faculty opponent: Sören Schlichting

To be presented, with the permission of the Faculty of Science of Lund University, for public criticism in Lundmarksalen at the Department of Physics on Friday the 27th of October 2023 at 10:00.

Organization
LUND UNIVERSITY

Department of Physics
Professorsgatan 1
SE–223 63 LUND
Sweden

Document name
DOCTORAL DISSERTATION

Date of disputation
2023-10-27

Sponsoring organization

Author(s)
Robin Törnkvist

Title and subtitle
ALPACA - A kinetic theory Monte Carlo event generator for heavy ion collisions

Abstract
Recent measurements of collective effect-like signals in small collision systems has highlighted the need for new models to explain these phenomena. One good candidate for such a model is the AMY QCD effective kinetic theory, which is valid for systems in- and out-of-equilibrium. This thesis is a collection of four papers which all investigate how to apply AMY kinetic theory to explain the evolution of small and large collision systems. In Paper I an analytical approach is used to extract collective flow coefficients from the kinetic theory. Paper II-IV then show the main work of the thesis, an implementation of the kinetic theory in the form of an event generator called Alpaca, as well as applications of this event generator to different systems.

Paper I presents results derived from the single-hit approximation of AMY kinetic theory looking specifically at the energy flow response to initial geometrical deformations in a purely gluonic system. It results in a scaling formula for the collective flow coefficients, and a proof-of-concept study of the flow response for small collision systems, which gives results that are correct in order of magnitude.

Paper II presents the main work of the thesis, the Monte Carlo event generator Alpaca (AMY Lorentz invariant PArton CAscade). The details of how the event generator is implemented to faithfully reproduce the dynamics of AMY kinetic theory are discussed, and a validation of the framework in the case of an infinite thermal equilibrium is shown.

Paper III show how different systems thermalize and isotropize in Alpaca. Two different scenarios are analyzed; an overoccupied thermal system for thermalization, and isoptropization for anisoptropic Color Glass Condensate-like initial conditions. It is found that the system thermalizes correctly for the overoccupied case, compared to known analytical results.

Paper IV investigates collective flow in small systems using Color Glass Condensate-like initial conditions in Alpaca. Comparisons between the single-hit approach of Paper I and Alpaca are made, and the details of the difference between first-hit, single-hit and all-hit are shown and discussed.

Key words
ALPACA, QCD effective kinetic theory, event generators, heavy-ion collisions, proton-proton collisions, small system collectivity, phenomenology

Classification system and/or index terms (if any)

Supplementary bibliographical information

Language
English

ISSN and key title

ISBN
978-91-8039-817-6 (print)
978-91-8039-818-3 (pdf)

Recipient's notes

Number of pages
195

Price

Security classification

Signature _____ Date 2023-09-12

ALPACA - A kinetic theory Monte Carlo event generator for heavy ion collisions

by Robin Törnkvist

LUND
UNIVERSITY

A doctoral thesis at a university in Sweden takes either the form of a single, cohesive research study (monograph) or a summary of research papers (compilation thesis), which the doctoral student has written alone or together with one or several other author(s).

In the latter case the thesis consists of two parts. An introductory text puts the research work into context and summarizes the main points of the papers. Then, the research publications themselves are reproduced, together with a description of the individual contributions of the authors. The research papers may either have been already published or are manuscripts at various stages (in press, submitted, or in draft).

Cover illustration front: Alpaca at Bosjökloster, 2023.

Funding information: This work is part of a project that has received funding from the European Research Council (ERC) under the European Union's Horizon 2020 research and innovation programme (Grant agreement No. 803183, collectiveQCD).

Faculty of Science, Department of Physics

ISBN: 978-91-8039-817-6 (print)
ISBN: 978-91-8039-818-3 (pdf)

Printed in Sweden by Media-Tryck, Lund University, Lund 2023

Till Nathalie och Elsie

Contents

Acknowledgements

First and foremost, I would like to thank my supervisor Korinna Zapp, for giving me the opportunity to work within the field of physics phenomenology, which was my goal after I was done with my masters thesis. I am very grateful for your endless patience and effort in guiding me through my PhD, and introducing me to kinetic theory, event generators, heavy ion physics and all other relevant and interesting physics that is contained in this thesis. Your supervision has been of invaluable help to me, and I look forward to further collaboration during my coming Postdoc. Also a thanks to my second supervisor, Leif Lönnblad, for very useful help and feedback during my PhD.

I would also like to thank my collaborators from my short term visit at CERN, Aleksi Kurkela and Aleksas Mazeliauskas. Working with you on my first article for this PhD taught me a lot, both about physics and how to work efficiently in a research project. A special thanks to Aleksas for our regular zoom-meetings during the COVID-19 pandemic, where you, with much patience helped me with my code and calculations.

A thank you to Christian Bierlich for proofreading this thesis and providing very helpful feedback which helped shape this thesis to its current state. Also a thank you to Timea Vitos for proofreading and helping with the popular summary in Swedish.

To all my fellow (at some point) PhD students (in no particular order); Marius, Chiara, Mattias, Emil, Timea, Nils, Leif, Andrew, Joel, Torbjörn, Smita, Astrid, Mårten, thank you for all the interesting discussions, social events, fikas, word of the day, etc. You have all made it very fun to work at the department. Thank you also to all the Postdocs that have come and gone since I started here, with a special mention to Jarkko, you have all also contributed a lot to this.

I would also like to thank my bachelor's and master's supervisors from Umeå University, Per Åhag and Michael Bradley. Per introduced me to how incredibly interesting and demanding pure math can be, and his lectures, supervision and discussions has set in motion what I believe will be a life long interest in pure mathematics (and also opened the door to philosophy). Michaels physics lectures are one of the main reasons that I decided to pursue a further career in physics, and the supervision and discussions during my masters project further strengthened this decision.

All my family up north of course also deserves a special thanks for all their support over the years, especially my parents and my sister Betty. Thank you for all the dinners, movie nights and fun dog-walks.

Also my friends from before academia deserve a thanks. This goes especially for Hampus and Olof; thank you for always being available for fun discussions, a beer, a movie and some video games.

Finally, my biggest thanks goes to my partner Nathalie and our daughter Elsie. Coming home to you every day is my greatest motivation, and I am incredibly lucky to have you both in my life.

List of publications

This thesis is based on the following publications:

I **Collective flow in single-hit QCD kinetic theory**

Aleksi Kurkela, Aleksas Mazeliauskas, **Robin Törnkvist**
JHEP **11** 216 (2021)
e-print: `arXiv:2104.08179 [hep-th]`

II **AMY Lorentz invariant parton cascade - the thermal equilibrium case**

Aleksi Kurkela, **Robin Törnkvist**, Korinna Zapp
Submitted to Eur.Phys.J.C
e-print: `arXiv:2211.15454 [hep-ph]`

III **Thermalization and isotropization in the AMY parton cascade Alpaca**

Robin Törnkvist, Korinna Zapp
To be submitted to Eur.Phys.J.C
e-print: `arXiv:2309.04413 [hep-ph]`

IV **Small systems and the single-hit approximation in the AMY parton cascade Alpaca**
Robin Törnkvist, Korinna Zapp
Submitted to Phys.Lett.B
e-print: `arXiv:2309.04458 [hep-ph]`

All papers are reproduced with the permission of their respective publisher, with minor stylistic changes in the layout and wording.

Populärvetenskaplig sammanfattning på svenska

Fysik är den samlade insatsen genom mänsklighetens historia att, på den mest fundamentala nivån, förstå och beskriva den objektiva verkligheten vi verkar befinna oss i.

Den grenen av fysik som arbetar med de mest fundamentala teorierna, vilken all annan fysik ska kunna härledas ifrån, har över tiden delat sig till två huvudfält; det *allra största* och det *allra minsta*. För det allra största ligger huvudfokus på att studera och beskriva händelser som sker över de största tid- och längdskalor vi kan mäta. Detta kan sträcka sig upp till till exempel Universums ålder (~ 13.8 miljarder år) samt sträckor som diametern på det observerbara Universum (~ 880 biljoner biljoner meter). För det allra minsta ligger fokus istället på de minsta beståndsdelarna av Universum, vilka kallas för *partiklar*. Här kan skalorna röra sig om till exempel protonradien ($\sim 0.84 \cdot 10^{-15}$ meter), eller till och med ännu mindre skalor när vi studerar fundamentala partiklar. Dessa beskriver vi som punktliknande, det vill säga att de (i viss mening) inte har någon storlek. I denna avhandling är vårat fokus på fysiken kring det allra minsta.

Fältet inom fysik för det allra minsta som vi beskrev ovan heter *partikelfysik*. För att beskriva objekt som existerar på dessa skalor förlitar vi oss på en teori som heter kvantfältteori, som beskriver partiklar med hjälp av matematiska fält. Användandet av kvantfältteori har resulterat i *Standardmodellen*, vilket är en av de mest framgångsrika vetenskapliga teorier som finns i dagsläget. Den beskriver egenskaperna av de fundamentala byggstenarna i Universum, vilka kallas *elementarpartiklar*, och hur dessa interagerar med varandra.

Alla förutsägelser av Standardmodellen, och alla andra partikelfysikmodeller, måste självklart testas och verifieras, och detta görs oftast vid experiment i partikelacceleratorer. Den mest kända av sådana acceleratorer är Large Hadron Collider vid CERN faciliteten i Genève, Schweiz. Här accelereras partiklar upp till väldigt höga energier för att sedan kollidera med varandra. Partiklarna som skapas av dessa kollisioner mäts sedan av detektorer placerade runt kollisionspunkten.

En typ av kollision som studeras på LHC är tungjonskollisioner. Dessa är väldigt energifyllda och omfattar många partiklar, både före och efter kollisionen. I dessa händelser uppnås temperaturer som möjliggör skapandet av *kvark-gluonplasma* snabbt efter kollisionen. Kvark-gluonplasmat är den äldsta formen av materia som har existerat i Universum, och det fyllde hela Universum runt 10^{-10} till 10^{-5} sekunder efter Big Bang. Genom sin existens i tungjonskollisioner har vi lyckats studera plasmat i detalj, och idag vet vi mycket om de egenskaper den uppvisar. Om vi undersöker andra änden av kollisionsspektrat dock, det vill säga små kollisionssystem som till exempel proton-proton, räknar vi inte med att kvark-gluonplasma ska skapas. Denna förväntning bygger på att dessa system inte är energitäta nog för att skapa plasmat utifrån de modellerna vi idag har att beskriva fenomenet med.

Nyligen har dock observationer av kvark-gluonplasma-liknande signaler i små kollisionssystem gjorts. Denna upptäckt utmanar vårt traditionella sätt att beskriva stora och små system med olika modeller, och det belyser en motsägelse i vår modell av den objektiva verkligheten som kräver utredning.

I de fyra artiklarna som avhandlingen innehåller, fokuserar vi på att bidra till att reda ut detta problem. Vi fokuserar på en kvantkromodynamisk effektiv kinetisk teori som en potentiell lösning för att förklara de uppmätta effekterna i små kollisionssystem. I den första publikationen i denna avhandling gör vi den förenklande uppskattningen att partiklar endast får kollidera en gång från att de ursprungligen skapas. Detta tillåter oss att numeriskt extrahera en specifik kvark-gluonplasma-liknande effekt från den kinetiska teorin. Den andra publikationen presenterar denna avhandlingens huvudarbete; programmet Alpaca. I den andra artikeln diskuterar vi detaljerna av denna implementation, samt verifierar att implementationen är korrekt. I de sista två artiklarna använder vi Alpaca för att studera mer specifika händelser och fenomen.

Popular summary in English

The science of *physics* is the collected effort throughout the history of humanity to, on the most fundamental level, make sense of the objective reality we seem to find ourselves in.

The branch of physics that deal with the most fundamental physical theories, from which everything else in physics should follow, has over time separated into two main fields; the *very large* and the *very small*. For the very large, the main focus is the study of events that take place over largest time and distance scales we can measure. This can range up to e.g. the age of Universe (~ 13.8 billion years), and distances like the diameter of the observable Universe (~ 880 trillion trillion meters). For the very small, the focus is instead the smallest constituents of the Universe, also known as particles. Here, the distance scales can concern e.g. the radius of a proton ($\sim 0.84{\cdot}10^{-15}$ meter), or even smaller when looking at fundamental particles which are considered pointlike, meaning (in some sense) that they have no size. In this thesis, the study of the very small will be our focus.

The field of the very small is known as *particle physics*. To describe the objects that exists within these scales we rely on a theory called Quantum Field Theory (QFT), which described particles by using mathematical fields. The use of QFT has resulted in the *Standard Model*, which is one of our most successfully scientific theories to this day. It describes the properties of the most fundamental building blocks of the Universe, known as *elementary particles*, and the way they interact with each other.

The predictions of the Standard Model, and other particle physics models, must of course be tested and verified, and this is most often done in experiments at particle accelerators. The most famous example of such is the Large Hadron Collider (LHC) at CERN in Geneva, Switzerland. Here, particles are accelerated to very large energies and then set to collide with each other. The particles that results from these collisions are then measured by detectors placed around the collisions.

One type of collisions that are being studied at the LHC are heavy ion collisions. These are highly energetic events which include many particles, both in and after the collisions. The collisions also become so hot so that a liquid known as the *Quark Gluon Plasma* (QGP) is formed right after the heavy ions have collided. The QGP is the oldest form of matter that existed in the Universe, filling the whole Universe around 10^{-10} to 10^{-5} seconds after the Big Bang. Through its existences in heavy ion collisions we have been able to study it in detail, and known much about the behaviour it exhibits. In contrast to this, looking at small collision systems like proton-proton, we do not (traditionally) expect any QGP to be formed since those systems are not dense enough.

Recently though, there have been observations of QGP-like signals in small collision systems. This has challenged the current paradigm of modelling small and large collision systems in very different ways, and it is highlighting a contradiction in our model of objective reality, which needs to be resolved.

The work presented in this thesis aims to contribute to resolve this issue. We focus on a QCD effective kinetic theory as a possible explanation of the observed phenomenon in

small collision system. In the first publication of the thesis we assume the simplifying condition that particles are only allowed to scatter once during an event. This allows us to extract one particular QGP signal, known as collective energy flow, numerically from the QCD effective kinetic theory. The second paper presents the main work of the thesis, Alpaca, which is an event generator that encodes the QCD effective kinetic theory. Event generators are tools that simulate particle collisions using numerical methods, and our implementation of this event generator is such that the dynamics of the system resulting from the collisions follows the QCD effective kinetic theory. In the second paper we discuss the details of the implementation as well as validate the model in a simpler setting. In the last two papers of the thesis, we then use Alpaca to look at more interesting scenarios.

Introduction

This thesis is the culmination of the work I have done since starting my PhD in Lund, and is centered around different implementations of the QCD effective kinetic theory introduced by P. Arnold, G. Moore and L. Yaffe (AMY) in Ref. [1]. Before I venture into the actual work of the thesis though, I would like to present a brief overview of my philosophical motivation for pursuing physics. Bear in mind that what is presented in this subsection is just my attempt at explaining *why I am doing physics*. The arguments involved represent my current best understanding of the topic, and as any philosophical arguments they would surely benefit from further discussion. However, the validity of the actual physics results presented later in this thesis bears no weight on these arguments.

For me it all starts with a simple question: how can we determine what objective reality, assuming that such a thing exists, is? The answer turns out to be a bit more complicated than the question itself, as it sets in motion a spiral of new questions. To answer these questions, we first need to decide on which game rules we should use to evaluate the validity of any answer to any following questions moving forward. As far as game rules go, I know of non-other as rigorously developed and intuitively preferable as *logic* (and so also by extension: mathematics).

Since logic now puts us in the realm of definitions, axioms and implications, it is suitable to pick a proper definition of what objective truth is, in terms of our models describing objective reality. As we, in a fundamental sense, only have access to our own subjective reality, I have always favored a version inspired by the one found in Ref. [2] concerning subjective and objective standpoints, which goes as follows.

A view or form of thought is more objective than another if it relies less on the subjective experience of the individual.

With this definition at hand we are now ready to describe objective reality. However, for purely pragmatic reasons I constrict us further and impose one more axiom, namely that any theory we construct should describe *physical* objective reality. This means that what it describes, should correspond to what we experience through sensory perception. This is a subset of objective truths, in which it has proved favorable[1] to assume that there exists *one* correct model[2]. This as opposed to the remainder of objective truths, denoted

[1] If one considers our knowledge of physics favorable, which I personally do.
[2] Or more specifically; *one equivalence class* of correct models.

abstract truths, like mathematical models where one can find an infinite number of true and consistent models[3]. We will still utilize the abstract truths found in the mathematics derived from Zermelo–Fraenkel set theory (with or without the Axiom of Choice[4]) to construct our models, but once we assume that an object in our model should correspond to a *physical* object, further verification than just logical consistency is required. Hence, with the extra axiom of describing physical truths, we have left the realms of philosophy and pure mathematics and arrived at the doorstep of physics.

The science of physics contains many branches, but if one wants to stay as close to the fundamental part of the theory as possible, one must look at the very largest (i.e. time and space) or smallest (i.e. particles and fields) scales. Though I find them both fascinating, I have always favored the reductionist approach of fundamentally explaining everything by looking at its smallest constituents, which inevitably lead me to particle physics.

The arguments outlined above of how to best describe objective reality are of course only a (very) simplified beginning. In e.g. the field of physics many great minds have refined our methods over the years, and we have further imposed philosophical concepts (and active discussion about the validity and reasonability of these concepts) to guide us through our exploration of objective reality such as e.g. the scientific method and the relaying of sensory perception to constructed detectors.

So to summarize; for me it starts with one simple question about how to determine what objective reality is. The answers to this question then inevitably leads me to physics, our best tool/language/model for rigorously describing the objective reality we seem to find ourselves in.

Now when the method of describing objective reality and which field to study has been decided, the next question is, *what* is there to do within this field? Staying true to the choice of logic as the most fundamental game rule it follows straightforwardly that: ex falso quodlibet, meaning "from falsehood, anything", or simply put, one contradiction and you're out. When contradictions become apparent, we cannot trust the fundamental assumptions of our descriptions anymore, and any kind of real progress in any theory or model affected is in some sense halted. Hence, it is of crucial importance to resolve any contradiction that appears in our theory. The contradiction in particle physics that has caught my interest is the one of *recent observations of collective-like behaviour in small systems*. This contradiction and my effort to contribute to resolve it motivates all the work presented in this thesis, and it will be explained and discussed in detail as follows.

In Section 1 we start by giving an overview of the theoretical background needed to understand the contradiction we aim to solve. We begin by explaining the foundation of modern particle physics; the Standard Model. We then move on to discuss the theory used to describe the dynamics caused by the strong force (which is the force of interest in our contradiction); quantum chromodynamics (QCD). It is followed by an overview of particle collisions and the field of phenomenology. This then ends the broader part of overview,

[3]Though depending on the complexity of the models, we might not be able to prove that they are consistent, which follows from Gödel's incompleteness theorems.

[4]I have yet to find one physical result which relies on the Axiom of Choice. Hence, *to the best of my knowledge*, it has no impact on physics, and so I leave it open to include it or not.

and from this we move on to our specific field of interest within particle physics.

In Section 2 we look at Heavy Ion Collisions and the collective behaviour we observe in those. We end this section by highlighting the open problem in particle physics which this thesis is centered around, namely the observed signals of collective like behaviour in small system. By small system we here mainly mean collisions between protons, and collective behaviour means that the remnants of the initial collision interact with each other after the collision has taken place, something our models predict should not happen in small systems. The specific collective behaviour in small systems we are mainly interested in for this thesis is that of collective flow. This is a phenomena where particles interact to cause asymmetries in the energy and particle number spectra, which is measured by the detectors around the collisions. At this point, we can ask the questions; *what theory* is a suitable candidate to explain these phenomenon, and *what methods* can we use to extract qualitative predictions and comparison to data from this theory. The answers to these questions are discussed in the two coming sections, starting with the latter question.

In Section 3 we look at the methods which we use to produce predictions and compare theory to data, namely Monte Carlo methods. We focus on showing how we can sample quantities from probability distributions, calculate multidimensional integrals and simulate decay processes. We end with a brief overview of Monte Carlo event generators, tools which are needed to get proper apple-to-apple comparisons between theory and data.

In Section 4 we give an overview of QCD effective kinetic theory, with the purpose of later showing how it can be used as a model which explains the signals of collective behaviour in small systems whilst also providing a smooth transition from small to large collision systems. After the overview about the relevant parts of the theory, we look at some specific applications which shows how it produces collective flow in small and large collision systems, namely the single-hit approximation which we implement in Paper I.

Finally, in Section 5, we tie it all together and present the main work of this thesis, the Monte Carlo event generator Alpaca, which is a Lorentz invariant parton cascade that encodes the AMY kinetic theory of QCD at high temperatures, using Monte Carlo methods. We provide an overview of how Alpaca functions, and look at how we have validated our implementation as well as some specific results we extract from it. The more technical details are left to Papers II-IV.

We then end the introduction with conclusions and outlook in Section 6 which includes a by a brief summary of Papers I-IV.

1 Particle physics

In this section we give a brief overview of the theoretical background needed to understand the main work of this thesis, which will be presented in the following sections. We start with the most fundamental model of particle physics; the *Standard Model*. Before we look at the Standard Model though, we note that it is common in particle physics to use *natural units*, and we will also adapt this convention throughout this thesis. This means that we

fix the speed of light c and the reduced Planck constant $\hbar$ such that $c = \hbar = 1$. With this convention, mass and momentum have units of energy E, and time and length have units of $1/E$.

1.1 The Standard Model

In particle physics, much is centered around the Standard Model. It is one of the most successful scientific theories we have, acting as a foundation of particle physics by describing the fundamental building blocks of the universe, and the forces through which they interact. The model is described in the language of Quantum Field Theory (QFT), which is a combination of two of the most remarkable theories discovered in the last century; quantum mechanics and special relativity. In QFT, particles are modelled as excitations of underlying quantum fields.

The Standard Model contains 17 *elementary particles*, as illustrated in Fig. 1. Out of these, 12 are *elementary fermions* which make up all matter. The fermions are further split into two groups, six *leptons* and six *quarks*. The remaining five particles are the *bosons*, with four of them being the *gauge bosons* responsible for three of the fundamental forces. These are the *photon* (γ) which mediates the electromagnetic force, the *gluon* (g) which mediates the strong force, and the $W^{\pm}$ and Z^0 bosons which mediate the weak nuclear interaction. The last boson is a *scalar boson*; the *Higgs boson*, responsible for giving mass to most of the fermions as well as the $W^{\pm}$ and Z^0 bosons. For each fermion there also exists a corresponding antiparticle. These particles have the same mass as the original, but opposite quantum number, i.e. the opposite value of some conserved quantity, as e.g. spin.

For each of the three fundamental forces described above we associate a *charge*. Particles with the same type of charge are then allowed to interact with each other, as well as with the mediators of that charge. This is illustrated in Fig. 1. The photon is the mediator of the electric charge, and so it interacts with all electrically charged particles. The electromagnetic force acts over large distances, and is responsible for most of the everyday phenomena we experience. The light from the sun that we see are photons within the visible spectrum hitting the retina in our eyes, the motion of the electrically charged particles in the electric current that fuels our mobile phones is mediated through photons, and so on. The theory of this force and its corresponding charged particles is called Quantum Electrodynamics (QED).

The $W^{\pm}$ and Z^0 mediate the weak force, and all fermions are charged under this. It is a short ranged force, acting under subatomic distances, and is partially responsible for radioactive decay.

Lastly, the gluon mediates the strong force. It only interacts with itself and the six quarks. The corresponding charge of these particles is called *color charge*. There are three types of color charge, red, green and blue. This force works in the opposite way of the electromagnetic force, which dampens over long distances. The strong force instead gets stronger over distance, which leads to a phenomenon known as *confinement*. This effect implies that color charged particles are bound over small distances by the strong force into color-neutral

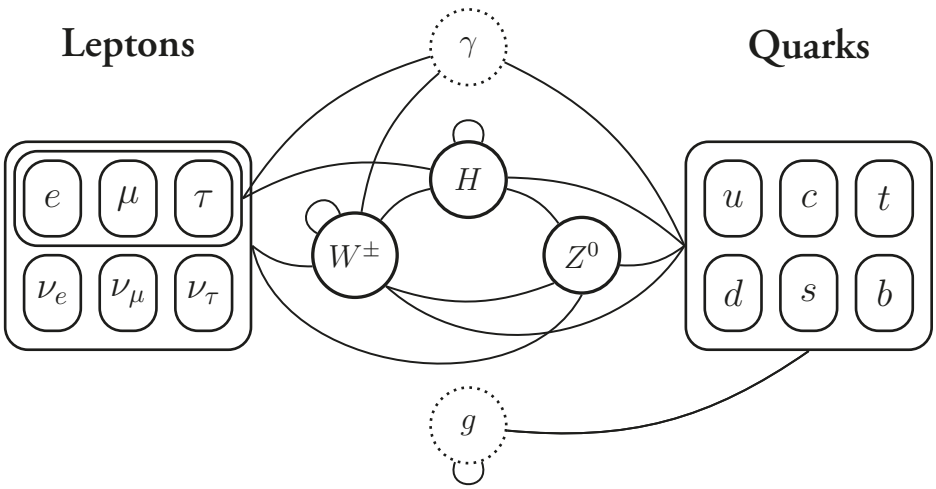

Figure 1: The elementary particle content of the Standard Model. Solid lines between different particles or particle groups indicate interactions. A dotted circle indicate that the boson is massless. The leptons split into two groups, where the neutrinos do not interact with the Higgs boson (H) or the photon (γ). All color charged particles interact with the gluon (g), all fermions interact with the $W^{\pm}$ and Z^0 bosons and all electrically charged particles interact with the photon.

configurations called hadrons, with e.g the most commonly known being the proton consisting of a uud combination of quarks, and the neutron consisting of udd. The theory of the strong force and color charged particles is called Quantum Chromodynamics (QCD) and is the main focus of this thesis. It will be discussed in further detail in Section 1.2.

The Standard Model has had many successes over the years, one famous case being the prediction, and following experimental verification, of the Higgs boson [3, 4]. It has also allowed for astonishingly precise comparisons between prediction and measurements, e.g. the anomalous magnetic moment of the electron where the predicted and measured value agree to the level of one part to 10 trillion (10^{13}) [5].

The Standard Model is not a complete description from which we can derive everything else in the Universe though. For example, it does not include the 4th fundamental forces, namely gravity. We have still not found a way to incorporate gravity in terms of elementary particles (though at quantum scales the force is so weak, in comparison to the other fundamental forces, that we can safely neglect it). On larger scales, where it becomes relevant it is well described by the theory of general relativity. In its original form the Standard Model also predicted the neutrinos to be massless, which has been shown not to be the case in recent experiments [6, 7]. This particular problem can be amended by simple extensions to the Standard Model though, e.g. through the Seesaw Mechanism. Overall, there is room

left for further improvement. Still, humanity has yet to create another model that has the amount of predictive power and experimental success, while also being this fundamental.

1.2 Quantum Chromodynamics

Out of the three fundamental forces in the Standard Model, the papers in this thesis concern only the strong force. Hence, a brief overview of QCD is needed before we proceed. QCD is a vast and mathematically intricate topic, though here we will keep it light and only focus on a few concepts relevant for understanding the rest of this thesis. Standard course literature is recommended for the reader looking for more details, such as e.g. Ref. [8].

As we saw in the last section, the elementary particles of interest in QCD are the gluon and 6 species of quarks: *up* (u), *down* (d), *charm* (c), *strange* (s), *top* (t) and *bottom* (b). The gluon mediates the strong force, and the associated charge is called a color charge. Hence, all the quarks are color charged. The gluon however, in contrast to the photon mediating the electroweak force, can interact with itself and is hence also color charged. There are three different colors, *red* (r), *green* (g) and *blue* (b)[5]. Every quark carries one of these colors, or a superposition of the three, and any species can carry any color. Since every charged particle has a corresponding anti-particle (the gluon being its own anti-particle) we also have anti-colors; *anti-red* ($\bar{r}$), *anti-green* ($\bar{g}$) and *anti-blue* ($\bar{b}$). The gluon carries a superposition of both color and anti-color.

The strong force acts in the opposite way of electromagnetic force; it decreases as distance decreases, as illustrated in Fig. 2. This property is known as *asymptotic freedom*. By looking at smaller and smaller distance scales, and hence larger and larger energy scales, the strong interaction between particle weakens to a point where the particle behaves as almost non-interacting. Going in the opposite direction and looking at large distance scales and lower energies, the force from the interaction increases. Hence, if we were to try and separate a quark and an anti-quark from each other by adding energy to the system to pull them apart, we would need to add even larger amounts of energy the further away they get. Due to the self-interaction of the gluon, the energy we add would eventually be transferred into creating a new quark closer to the original anti-quark, and a new anti-quark closer to the original quark. Thus, we end up with two new strongly bound pairs. This phenomenon is known as *color confinement*, and implies that quarks cannot exist in isolation.

In confinement, only color neutral combinations of quarks will produce a stable state. A color neutral state of quarks is called a *hadron*, and we separate the hadrons in two groups: *mesons* which contain a quark and an anti-quark, and *baryons* which contain three quarks (or three anti-quarks). For mesons, color singlet states are produced by combing an even number of colors with the corresponding anti-colors, e.g. $r\bar{r}$. For baryons, the color singlet state is e.g. of the form rgb or $\bar{r}\bar{g}\bar{b}$. States composed of more quarks, also known as exotic mesons or exotic baryons, are possible, but so far only tetraquarks, e.g.

[5]Note that this is just a naming convention. These colors have nothing to do with the colors red, green and blue that we experience in everyday life, which are due to photons propagating with corresponding frequencies in the visible spectrum of light.

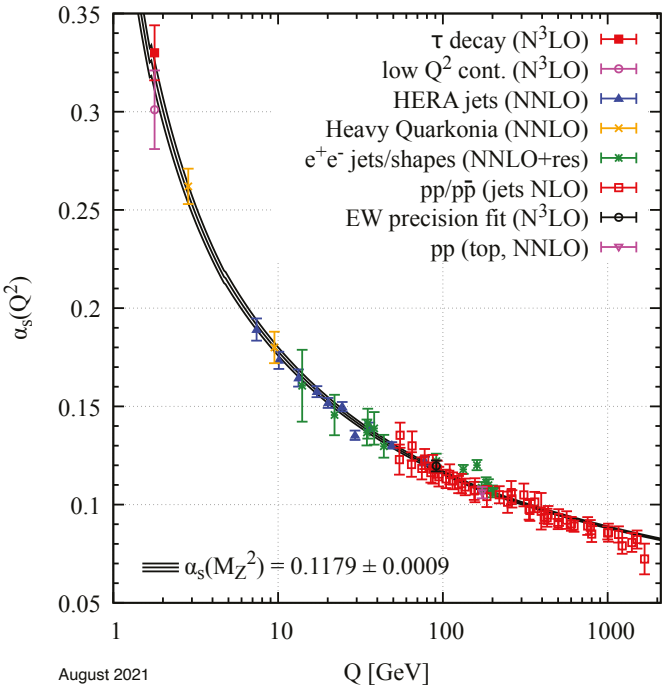

Figure 2: The QCD running coupling, α_s, evaluated at the energy scale of the Z boson, as a function of energy Q [9]. The solid lines correspond to the theoretical prediction, and the bars correspond to measurements of α_s through different methods.

$r\bar{r}b\bar{b}$ and pentaquarks, e.g. $rgbr\bar{r}$, have been observed. The particles that hadrons consist of are often referred to as *partons*.

1.3 Cross sections

A crucial component of quantum field theories such as QCD, which we will use frequently in this thesis, is the concept of cross sections, usually denoted σ. Cross sections have units of area, and for e.g. two pointlike particles it corresponds to the area transverse to the particles' relative motion in which they must meet for a scattering between them to occur. To show how we can derive cross sections, we start out on very general grounds by representing an initial state of incoming particles as $|\mathrm{i}\rangle$. In QFT we have what is known as an S-matrix, or the scattering matrix, which brings our initial state to a final state $|\mathrm{f}\rangle$,

$$|\mathrm{f}\rangle = \mathrm{S}|\mathrm{i}\rangle. \tag{1.1}$$

The modulus squared of the probability amplitude $|\langle \mathrm{f}|\mathrm{S}|\mathrm{i}\rangle|^2$ then corresponds to the probability density of starting with state $|\mathrm{i}\rangle$ and ending up with state $|\mathrm{f}\rangle$. By defining $\mathrm{S} = 1 + i\mathrm{T}$

we collect the process which has no interaction in the first term, 1, and the remaining amplitude of going from our initial to final state then allows us to define $\mathcal{M}(\mathrm{i} \to \mathrm{f})$ through

$$\langle \mathrm{f}|i\mathrm{T}|\mathrm{i}\rangle = (2\pi)^4 \delta^{(4)}(P_\mathrm{i} - P_\mathrm{f}) i\mathcal{M}(\mathrm{i} \to \mathrm{f}) \tag{1.2}$$

where P_i and P_f corresponds to the sum of the initial and final four-momentum respectively, and so the Dirac delta ensures four-momentum conservation of the process. Our newly defined quantity $\mathcal{M}$ is called the *matrix element* and captures the dynamics of the interaction. It is often expressed as Feynmann diagrams, see Fig. 3 for examples. In this thesis we are only concerned with cross sections for $2 \to n$ process, i.e. 2 incoming and n outgoing particles, and using the matrix element, we can now express the differential cross-section for such a process as

$$\frac{d\sigma(p_A, p_B \to p_1 \dots p_n)}{d\Phi_n} = \frac{|\mathcal{M}(p_A, p_B \to p_1 \dots p_n)|^2}{4\sqrt{(p_A p_B)^2 - (2m_A m_B)^2}} \prod_{i=0}^{n} [1 \pm f_i(p_i)] \tag{1.3}$$

where p_A, p_B and m_A, m_B are the momenta and masses of the incoming particles. The square root factor is known as the flux factor, and it normalizes the differential cross-section w.r.t. the incoming particle flux. The factors within the square bracket correspond to Bose enhancement and Pauli blocking (correspondingly $+$ for bosons and $-$ for fermions). The factor $d\Phi_2$ is the Lorentz invariant phase space measure for n outgoing particles. It corresponds to an infinitesimal volume in the outgoing phase space and is defined as

$$d\Phi_n = (2\pi)^4 \delta^{(4)} \left(P_A + P_B - \sum_i P_i \right) \prod_{i=1}^{n} \frac{1}{(2\pi)^3} d^4 p_i \delta(p_i^2 - m_i^2) \Theta(E_i), \tag{1.4}$$

where the first Dirac delta enforces total four-momentum conservation of the outgoing configuration, the second enforces the on-shell condition for each outgoing particle, and the Heaviside step function ensure that each outgoing particle has positive energy. Hence, only the outgoing configurations, where these conditions are met, contribute to the volume.

Combining the pieces presented above, we arrive at our total cross-section for $2 \to n$ processes by integrating over all allowed configurations in the outgoing phase space,

$$\sigma = \int \frac{d\sigma}{d\Phi_n} d\Phi_n. \tag{1.5}$$

The $2 \to n$ cross-section, and how to relate it to our model of choice, is a central part in our implementation of Alpaca, which we will discuss in more detail in Section 5 (and in even greater detail in Paper II).

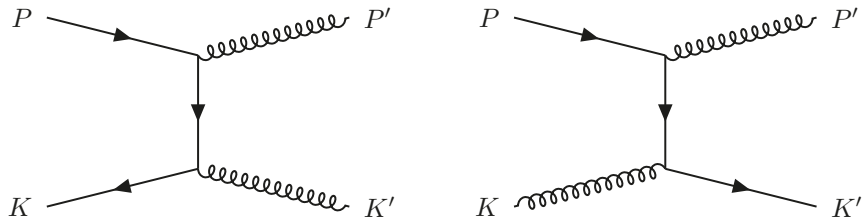

Figure 3: Examples of two different Feynmann diagrams with two incoming particles with four-momentum P and K interacting, resulting in two outgoing particles with P' and K'. Solid lines corresponds to fermions and anti-fermions, curly lines corresponds to gluons. Time can be viewed as going from left to right. Particles with arrows moving against the time direction corresponds to anti-particles. Left: $q\bar{q} \to gg$. Right: $qg \to gq$.

1.4 Particle collisions and phenomenology

Up until now we have only talked about our theories and models for describing objective reality, but how do we actually verify what our theories predict? The answer to this, which might seem obvious, is through experiments.

As we saw in Section 1.2, if we want to study fundamental properties of quarks, and not hadrons, we need to break confinement, meaning that we want to decouple the quarks that are bound by the strong force as hadrons. To this end, particle accelerators exists. In those, different particles are accelerated to large energies and then set to collide, after which the products of the collision are measured. The most famous particle accelerator is the Large Hadron Collider (LHC) at CERN in Geneva, Switzerland. It is the largest and most powerful particle accelerator that exists, accelerating e.g. protons through a circular loop up to energies of 6.8 TeV per proton. CERN was founded as an international collaboration between 12 countries in 1954 and has grown to now have 23 member states. It has been responsible for numerous successful discoveries in particle physics since it was founded, e.g. the discovery of the Higgs boson [3, 4], but has also produced applications outside of particle physics which have had a great impact on the world, e.g. the world wide web.

At the LHC, the main focus of the experiments is colliding protons with protons ($\mathrm{p} + \mathrm{p}$), and heavy ions with heavy ions ($\mathrm{A} + \mathrm{A}$). Proton collisions with heavy ions ($\mathrm{p} + \mathrm{A}$) are also investigated. We will look into the theory and experimental outcome of these processes in more detail in Section 2, but as a brief overview one can summarize these kinds of events as highly energetic events where we can have hundreds (and even thousands) of final state particles from the initial collisions.

As both experiment and theory has become more advanced over the years, the gap between the two has grown to a point where a whole new field has developed between them: phenomenology. While technically a part of theoretical physics, its purpose is to bridge the gap between theory and experiment. In phenomenology, the goal is to take current theories and make quantitative predictions from these, which can then be used by experi-

mentalists. Since the number of particles in the final states of particle collisions is so large, and our theories are probabilistic in nature, it is often impossible to do this by direct analytic calculations. Instead the development and use of numerical methods are often heavily involved. One of the main tools that a phenomenologist like myself develop and use, and which is a main theme of this thesis, are *Monte Carlo event generators*, which we will look at in more detail in Section 3. Before we move to such technical details though, we will in the next section introduce the specific field within particle physics which we are interested in: heavy ion physics.

2 Heavy ion collisions

In this section we finally arrive at the specific field within particle physics, where we will find the sought after contradiction, that this thesis is centered around; the collisions of heavy ions. These are highly energetic events which can involve thousands of final state particles that reach the detectors.

The way we model heavy ion collisions today started after the Relativistic Heavy Ion Collider (RHIC) in 2001 released early results of head-on collisions between gold ions ($\mathrm{Au} + \mathrm{Au}$) at an energy of 200 GeV per nucleon pair. These results indicated that most of the energy in the collisions was being deposited into a medium which could be described using hydrodynamics [10–13]. This new state of matter came to be called the Quark Gluon Plasma (QGP), and is a state where the partons are deconfined due to high energy density, and chiral symmetry is restored (see e.g. Refs. [14, 15] for an introduction and overview of the properties of the QGP). The formation of a QGP was expected on general grounds as a consequence of asymptotic freedom, predicted as early as the mid-seventies [16, 17]. It has, since its experimental discovery, been found that it behaves as a nearly perfect fluid, meaning it has a ratio of shear viscosity to entropy density close to the lower bound of theoretically allowed values, $\eta/s \sim 1/4\pi$ [18, 19]. The LHC later observed the same behaviour when colliding lead ions ($\mathrm{Pb} + \mathrm{Pb}$) at higher energies, up to 5.02 TeV per nucleon pair [20, 21].

One of the main reasons to study heavy ion collisions today is to study the QGP. By probing the QGP at lower length scales (i.e. higher energy scales, looking at e.g. high energy particles passing through the medium) we can gain insights about almost free quarks and gluons, due to the deconfined state of the particles in the QGP. The QGP is also the first form of matter to form in the universe, and the only matter to exist within a microsecond after the Big Bang. Hence, by studying the QGP that appear in heavy ion collisions we can learn more about the very early universe, see e.g. Ref. [22].

2.1 Formalism

Before we look at the details of an heavy ion collision, we first need to introduce the formalism which is used when looking at heavy ion collisions. Most commonly, we align our axes so that the z-direction is along the beam pipe, i.e. making our two beams move along

the z-axis. Hence, $\mathbf{x}_\perp$ and $\mathbf{p}_\perp$ describe the spatial and momentum components in the transverse direction to the beam. Next, we need to introduce two new quantities; *rapidity* (y) and *pseudorapidity* (η). The rapidity is used at relativistic energies as a measure related to velocity, and is defined as

$$y = \frac{1}{2}\ln\left(\frac{E+p_z}{E-p_z}\right) = \frac{1}{2}\ln\left(\frac{\sqrt{m^2+p^2}+p_z}{\sqrt{m^2+p^2}-p_z}\right), \tag{2.1}$$

for some particle with 4-momentum $P^\mu = (E, p_x, p_y, p_z)$ and rest mass m. It has the benefit of being additive under Lorentz boosts in the beam direction (along the z-axis). It does however introduce some trouble in terms of measurements, since we need to know both the total momentum and relativistic mass of the particle. To remedy this, we can instead look at the pseudorapidity

$$\eta = \frac{1}{2}\ln\left(\frac{p+p_z}{p-p_z}\right) = -\ln\left(\tan\frac{\theta_\mathbf{p}}{2}\right) \tag{2.2}$$

where $\theta_\mathbf{p}$ is the polar angle w.r.t. to the beam direction of the momentum. For large enough transverse momentum, $m \ll p_\perp$ (or equivalently when the particle is effectively massless), we have that $\eta \approx y$.

With these definitions at hand we are ready to look at the details of a heavy ion collision.

2.2 Timeline

The timeline of a heavy ion collision is illustrated in Fig. 4 (see e.g. Ref. [23] for a more in-depth discussion). Before colliding, the two ions effectively have the shape of Lorentz contracted discs, which for Pb and Au have a diameter around 14 fm ($14 \cdot 10^{-15}$ meter). The discs consists of a large number of quarks and anti-quarks, where which act as sources for strong color fields, i.e. gluons, spanning almost completely in the transverse direction. The area density of partons is not uniform, and fluctuates from nucleus to nucleus.

When the discs collide, many interactions occur between the partons of the discs. Most of these interactions involve a small energy transfer, also known as *soft interactions*, but a fraction involve large energy transfers, known as *hard interactions*, and these partons will later lead to the production of collections of outgoing hadrons with large transverse momenta (also known as jets). During the initial collision some color charge exchange will occur between the discs. This results in color fields which stretch out longitudinally to fill the space between the discs, and these will quickly decay into $q\bar{q}$ pairs and gluons. These partons form a highly anisotropic system which expands at nearly the speed of light longitudinally, and starts to expand transversely as well. This stage is known as the pre-equilibrium stage. Any interaction between the remnants of the initial collision from this point forward is defined as *final state interactions*.

After around 1 fm of time, the system left between the receding discs has thermalized up to a point where it is well described by viscous hydrodynamics. The nearly perfect fluid

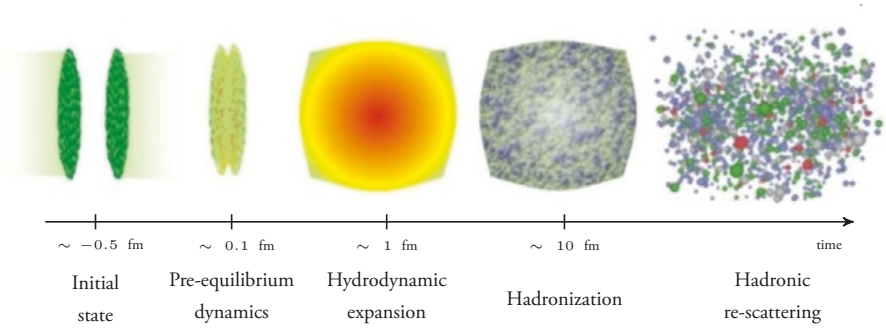

Figure 4: Timeline of a heavy ion collision. Starting out in the initial state are two Lorentz contracted discs moving towards each other along the beam direction. After they collide there is a short period of pre-equilibrium dynamics where the remnants of the collision form a rapidly expanding, highly anisotroppic system. Next, due to the final state interactions between the remnants, the system thermalizes into an expanding, deconfined quark gluon plasma. It expands until it has cooled off enough for confinement to act again, hadronizing the partons. The hadrons then re-scatter for a while up until a point where they just free stream to the detectors. Image courtesy of Steffen A. Bass.

that is formed is the QGP we discussed in the beginning of this section. It expands due to the initial pressure up until a point where it has cooled enough that the partons become confined again, after around 10 fm. This is called hadronization, as the partons in the QGP combine to create hadrons. The hadrons then stream out towards the detectors, and can rescatter with each other up until a point which is called kinetic freeze-out. After the kinetic freeze-out each hadron has its final state momentum, which will then be measured by the detectors.

Out of the different stages of a heavy ion collision outlined above, we are most interested in the pre-equilibrum and QGP stages, which through the final state interactions produces an effect known as *collective behaviour*.

2.3 Collectivity

The final state interactions in heavy ion collisions which causes the fluid like behaviour give rise to many measurable effects, which are usually referred to as *collective behaviour*. We will focus on one of these effects, which is at the center of explaining the open question we will discuss in the end of this section, namely *collective flow*.

There are two types of flow; particle number flow and energy flow. The former is the correlation in the number of particles moving in certain directions. The latter is the correlation in energy moving in certain directions, this is illustrated in Fig. 5. In this figure we see the measured energy output, shown as red towers for electromagnetic energy and blue towers for hadronic energy. The energy is clearly asymmetrically distributed, with correlations on

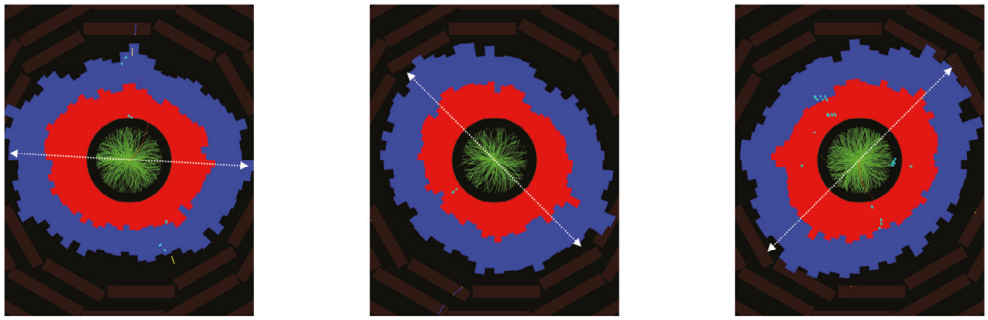

Figure 5: Signs of (elliptic) collective flow from $\mathrm{Pb} + \mathrm{Pb}$-events at CMS, in the direction transverse to the beam axis. The red bars indicate measured electromagnetic energy, and the blue bars hadronic energy. A clear correlation between opposite sides can be seen. Image courtesy of Gunther M. Roland (CMS).

opposite sides of the detector. Looking back at our initial colliding discs, we see that if they do not completely overlap when colliding, the overlapping area will be of a lenticular (almond) shape. This will cause anisotropies in the pressure of the QGP, which in turn causes anisotropies in the expansion velocity which are then reflected in the final state transverse momentum distribution. For a perfect lenticular shape as initial conditions, we would get what is called elliptic flow. However, the energy and parton density is not uniform in the initial discs, so the inital condition will not be a uniform lenticular shape. This causes further anisotropy that contributes to higher orders of flow.

The particle number flow is defined as [24, 25]

$$\frac{dN}{d\phi_{\mathbf{p}}} = \frac{\langle N \rangle}{2\pi}\left(1 + 2\sum_{n=1}^{\infty} v_n \cos[n(\phi_{\mathbf{p}} - \psi_n)]\right) \tag{2.3}$$

where $\phi_{\mathbf{p}}$ is the azimuthal angle of the momentum, $\langle N \rangle$ is the mean number of particles per event, and ψ_n is the mean angle of the n-th reaction plane[6]. The coefficients v_n are called the *flow coefficients*, where $n = 2$ corresponds to elliptic flow, $n = 3$ triangular flow, etc. They are in general functions of the transverse momentum, $p_\perp$, as well as the rapidity y, and are for the particle flow given by

$$v_n(p_\perp, y) = \langle\langle \cos[n(\phi_{\mathbf{p}} - \psi_n)]\rangle\rangle \tag{2.4}$$

where the double angular brackets indicate the average value over all particles in an event, and average over all events.

[6]The reaction plane for an event is a plane aligned with the lenticular shape of the initial collision, and the reaction plane angle is the angle between the x-axis of the reaction plane and the x-axis of the reference detector in the lab frame. It is not possible to measure this directly though, and an approximation known as the event plane is used instead, see e.g. Ref. [26] for details.

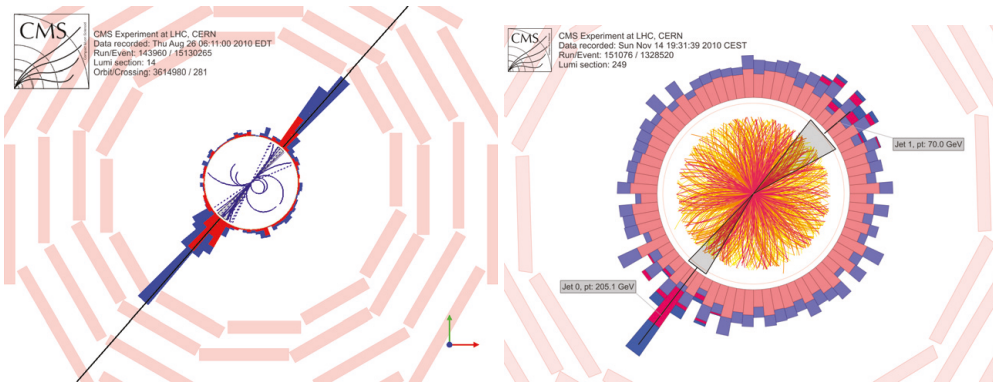

Figure 6: Energy measurements, in the direction transverse to the beam axis, of small and large collisions at CMS illustrating jets and jet quenching. The red bars correspond electromagnetic energy, and the blue bars hadronic energy. Left: $\mathrm{p}+\mathrm{p}$-event, jets are back to back with similar energy output on both sides, no clear sign of jet quenching. Image courtesy of CMS. Right: $\mathrm{Pb}+\mathrm{Pb}$, cones are not symmetrical in angle or amplitude in energy output, as an effect of jet quenching [27].

The energy flow is defined similarly as,

$$\frac{dE_\perp}{d\eta d\phi_{\mathbf{p}}} = \frac{dE_\perp}{2\pi d\eta}\left(1 + 2\sum_{n=1}^{\infty} v_n \cos[n(\phi_{\mathbf{p}} - \psi_n)]\right), \tag{2.5}$$

where once again v_n are the flow coefficients, $E_\perp$ is the tranverse energy and η is the pseudorapidity. This particular form of flow will later be our main focus in Paper I and IV.

2.3.1 Jet quenching

Apart from collective flow, the formation of a QGP also has other signatures that have been verified, with one of the most notable ones being centered around *jets*. A jet is, in broad terms, a collection of particle with high transverse energy, originating from the initial hard scatterings of the collisions. The original partons of the hard scattering will each create a parton shower, i.e. they radiate partons in a similar direction as they move out towards the detectors. This collection of partons form the shape of a cone outward from the initial collision, and the cones come in pairs, back-to-back since momentum is balanced in the initial hard scattering. An example of a pair of jets can be seen in the left part of Fig. 6. Here, two jets are formed back-to-back in a $\mathrm{p}+\mathrm{p}$ collision, with similar energy output as shown by the height of the bars, which indicate energy deposited in that direction.

The phenomenon of *jet quenching* is when highly energetic parton(s) traverse a medium and interact with it along the way. These final state interactions will cause the jet to loose energy to the medium, with the deposited energy mostly taking the form of many soft

particles with a large angular separation from the original jet. This can be seen by again looking at Fig. 6. In the left figure showing the $\mathrm{p}+\mathrm{p}$ event, we do not expect a medium and hence no jet quenching, so the jets are back-to-back with similar amplitude in energy output. In the right figure however, showing two jets in a $\mathrm{Pb}+\mathrm{Pb}$ event, we see that the two jets are no longer as symmetrical. They are not as back-to-back, the width of the cones now differ and the energy output is not symmetrical. This is due to the effects of jet quenching caused by the jets traversing the QGP that is formed.

Another noteworthy QGP signature, though not a part of the main focus of this thesis, is what is called *strangeness enhancement*, where an enhancement in the number of hadrons produced which contain multiple strange quarks has been measured, both in small and large collision systems [28].

2.4 Open questions: small and large systems

Now we are leaving the overview and background part of this thesis, and transition into something even more interesting: the open questions forming the current frontier of particle physics research [29]. As have been mentioned throughout this thesis, my main focus is to contribute to resolving the contradiction that has emerged from recent experimental measurements of small collisions systems, which show signs of collective behaviour. I will now explain in detail what I mean by this.

In the previous section we discussed collective behaviour, and how it is expected to appear in heavy ion collisions. The traditional view of small collision systems however, is maximally different from the one of heavy ions. Here, we have assumed that the colliding protons undergo an initial scattering, but we assume that the energy density of remnants of this scattering is not large enough to form a QGP. Hence, the remnants of the initial hard scattering produce independent vacuum showers, i.e. they stream towards the detectors while radiating other particles which moves in a similar direction. This continues up until a point of hadronization, and then free stream to the detector. Multiple other effects also contributes to the evolution of the system, like QCD effects from soft scatterings and electromagnetic QED effects, however, in this view collectivity is not possible, since we do not have any final state interactions. The vacuum showers evolve (mostly) independent of each other.

In Ref. [30] it was shown however, as shown in Fig. 7 that we can observe a clear ridge in 2-particle correlations in high multiplicity $\mathrm{p}+\mathrm{p}$ collisions, around $\Delta\phi = 0$ and large values of $\Delta\eta$. What this means is that there are long range correlations between particle pairs in these $\mathrm{p}+\mathrm{p}$ collisions. If there is collective flow in the system it would imply that there is a ridge along $\Delta\phi = 0$ for the 2-particle correlations. However, it would not be visible around $\Delta\eta = 0$ since the 2-particle correlations from jets are dominant there (see Fig. 7). It would, however, be visble as a ridge for larger $\Delta\eta$, i.e. long range correlations. The long range correlations are expected for heavy ion collisions where we assume that a QGP is formed, and even for $\mathrm{p}+\mathrm{Pb}$ collisions (which can also be seen in Fig. 7). But it is in clear contradiction to our traditional view of the small collisions systems having no final state interactions. Quantifying it in terms of the collective flow coefficients for elliptic flow, as

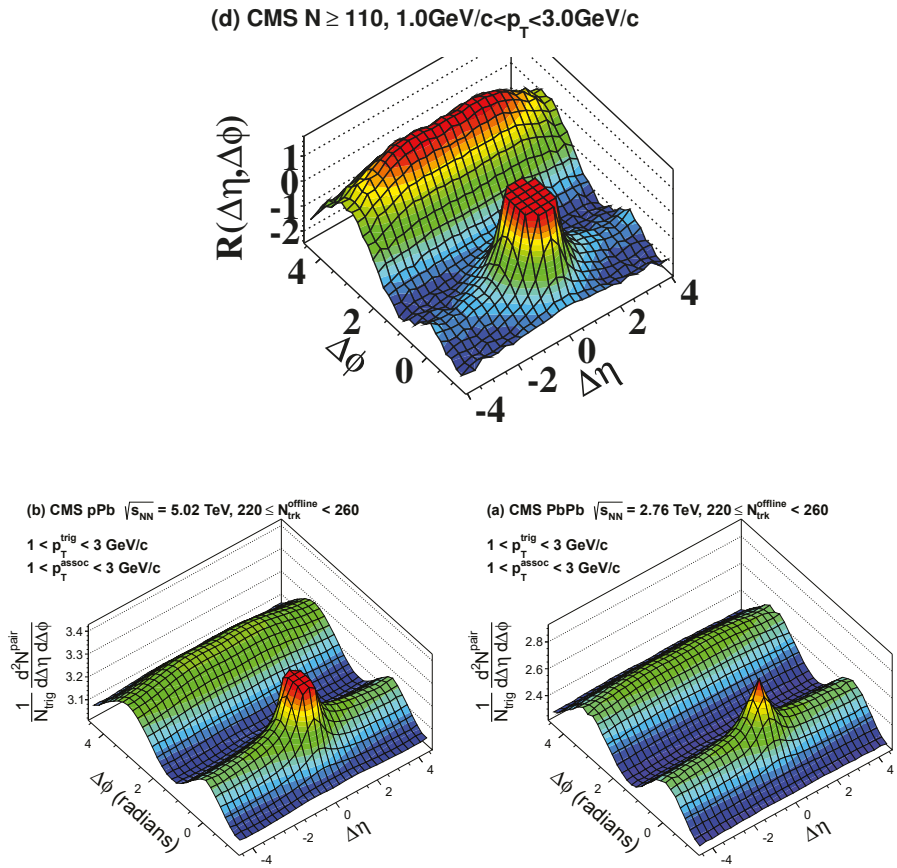

Figure 7: Plots of two-particle correlations as functions of relative azimuthal angle and relative pseudorapidity. Top: p + p [30]. Bottom: left is p + Pb and right is Pb + Pb [31].

shown in Fig. 8, we see a clear signal of elliptic flow for p + p collisions [32].

Now, one might naively think that since we observe signs of collective flow then our initial assumption about the system not being dense and energetic enough to form a QGP was wrong. However, the question gets more complex than this when we look at the other signs of collective effects, specifically jet quenching. This effect was first verified to be absent to any significant degree in d + Au (deuterium and gold collisions) [33–35], and later in the smaller collision systems by measuring single hadrons in p + Pb and Pb + Pb [36]. Since the formation of a QGP would also imply jet quenching, our question seem to have turned into something more complex than just: is there a QGP or not in p-p collisions?

What is described above is a clear contradiction between our traditional view of modelling small and large collision systems, and experimental data. What is needed to resolve this

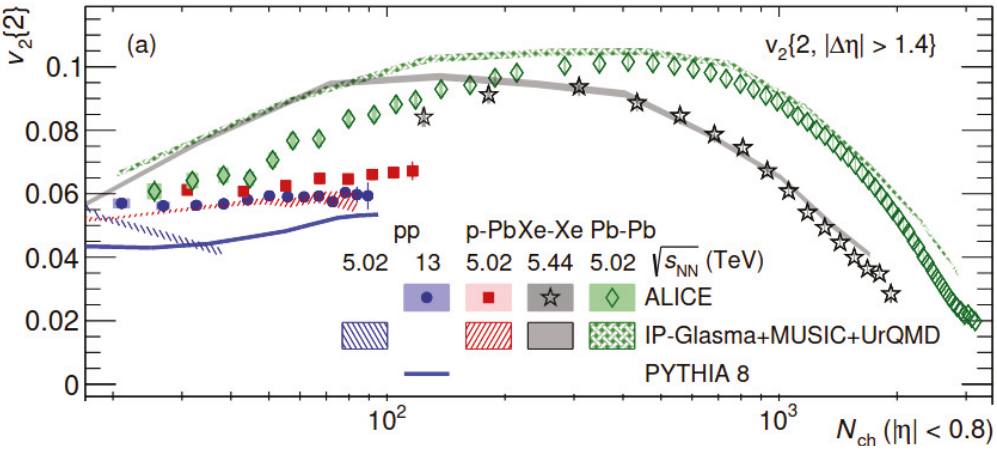

Figure 8: Elliptic flow coefficient for $\mathrm{p}+\mathrm{p}$, $\mathrm{p}+\mathrm{Pb}$, $\mathrm{Xe}+\mathrm{Xe}$ and $\mathrm{Pb}+\mathrm{Pb}$ as a function of charged particle multiplicity (average number of charged particles produced in the collision at mid pseudorapidity) measured by ALICE [32]. A clear signal of elliptic flow in the smallest collision system $\mathrm{p}+\mathrm{p}$ is shown.

is a new theory which can reproduce the experimental data of collective flow signals, but introduces no significant jet quenching in small systems. Also, the data indicate that the collective flow signals do not appear in a discrete way, but rather emerges smoothly as a function of system size, see Fig. 8 (with hopes that the future planned Oxygen-Oxygen run at the LHC will give new relevant information to further fill the gap in this spectrum [37]). Hence, it is also preferable if our theory can provide us with a smooth transition between small and large collision systems. This smooth transition must eventually take us back to a QGP where hydrodynamics is a viable model, as the system size increases. There are many different ongoing attempts to find solutions to these problems, with e.g. the string interaction models [38, 39] in Pythia [40] being some of the more notable ones.

Now that we have identified the contradiction of interest, and outlined what is needed in a theory to resolve it, we need to answer two questions; *what theory* do we find suitable to solve this problem, and *what methods* can we apply to that theory to gain qualitative predictions? We find that a possible answer to the first question is *QCD effective kinetic theory*, which is a highly suitable candidate, and we proceed to discuss it in detail in Section 4. Before we do that though, we will look at the answer to the second question, which is a numerical toolset known as *Monte Carlo methods*.

3 Monte Carlo methods

Our underlying framework in particle physics, quantum field theory, is not a measurably deterministic theory [7], instead we rely on probabilities. This poses certain challenges when we want to make predictions based on our theory, as we have to extract them from probability densities. We are also faced with the problem that many of the integrals we need to solve are multidimensional over possibly very large number of dimensions, often due to many particles with a 6-dimensional phase space each. The solutions to these problems are found in *Monte Carlo methods*. These are numerical methods which use repeated sampling of pseudo-random numbers[8] to solve numerical problems.

Monte Carlo methods play a central role in Paper I-IV, and in this section we will focus on giving a (somewhat) detailed overview the Monte Carlo methods that we have made use of the most. In order to keep it concise, we omit the proofs of the derivations in this section. These, and further discussions about the topic can be found in e.g. Ref. [40].

3.1 Sampling from probability distributions

First of all, our most commonly needed method is that of sampling discrete values from a distribution. This is most often used to sample particles' position and momentum from some initial distribution, but can also be used for e.g. sampling energy transfer in an elastic scattering. Given a probability distribution $f(x)$, normalized such that,

$$\int_{x_{\min}}^{x_{\max}} f(x)dx = 1 \tag{3.1}$$

the *cumulative distribution function* is defined as

$$C(y) = \int_{x_{\min}}^{y} f(x)dx \tag{3.2}$$

where $y \in [x_{\min}, x_{\max}]$. Hence, $C \in [0, 1]$, and so for any random number $R \in [0, 1]$ there is a corresponding y such that

$$C(y) = R. \tag{3.3}$$

[7] Though the theory itself is still deterministic, in the sense that the motion of the fields are bound deterministically from the equations of motions derived from the Lagrangian of the Standard Model. The seemingly nondeterministic behavior enter through the collapse of the wave function. This is what is defined to happen when a measurement takes place, i.e. when we measure something we force the probability distributions to single points, so it collapses to a Dirac delta function. Since we do not know how the collapse occurs in detail there are many unknowns which could cause the seemingly nondeterministic behaviour; our interpretation of the field itself, our definitions of e.g. "to *be* at position x with momentum p", the mechanics involved in the collapse of the wave field, etc. Hence, at our current knowledge of the theory the deterministic behaviour is not something we can access, though the theory still evolve in a deterministic manner.

[8] Pseudo-random numbers are numbers which pass as random given certain conditions.

Taking the inverse of this, we can sample y from the distribution f as

$$y = C^{-1}(R). \tag{3.4}$$

If the primitive function $F(x)$ of $f(x)$ is known, and also its inverse $F^{-1}(x)$, we can straight forwardly sample y from f as

$$y = F^{-1}\left(F(x_{\min}) + R[F(x_{\max}) - F_{x_{\min}}]\right) \tag{3.5}$$

where R is sampled uniformly between 0 and 1. Notice that in this last expression we have generalized our method slightly and removed the assumption that the distribution needs to be normalized to unity.

The sampling method above gives a straight forward way of sampling a quantity given it has a known and invertible primitive function. Often though, we deal with quite intricate probability distributions, and the primitive functions do not have a well defined inverse. This problem can be circumvented by finding an overestimate $g(x) \geq f(x)$, with a simple primitive function $G(x)$ and inverse primitive function $G^{-1}(x)$. The algorithm then goes as follows.

(i) Find simple $g(x) \geq f(x)$ with known primitive function $G(x)$ and inverse primitive function $G^{-1}(x)$.

(ii) Sample y from $g(x)$ following Eq. (3.5).

(iii) Sample new $R \in [0, 1]$ uniformly. If $R \leq f(y)/g(x)$ accept the value of y, otherwise reject it and cycle to (ii).

Following the algorithm outline above, one then ends up with a sample y from $f(x)$. The simplest case which is often available as an overestimate is a constant, e.g. $g(y) = f_{\max}$. This is known as *accept/reject* (or *hit-and-miss*) Monte Carlo. This is often not sufficient though, since it can lead to an excessive rejection rate. Hence, a non-constant $g(x)$ which follows $f(x)$ more closely so that one is preforming the sampling in the correct region, is preferable whenever it can be found. This is refered to as *importance sampling*, see Fig. 9 for an illustration of the process.

Another common scenario that occurs when sampling is that the distribution can be overestimated with a sum of functions, that is

$$f(x) \leq g(x) = \sum_i g_i(x). \tag{3.6}$$

We can then first select which i to use by the relative probabilities I_i, given by

$$I_i = \int_{x_{\min}}^{\max} g_i(x)dx. \tag{3.7}$$

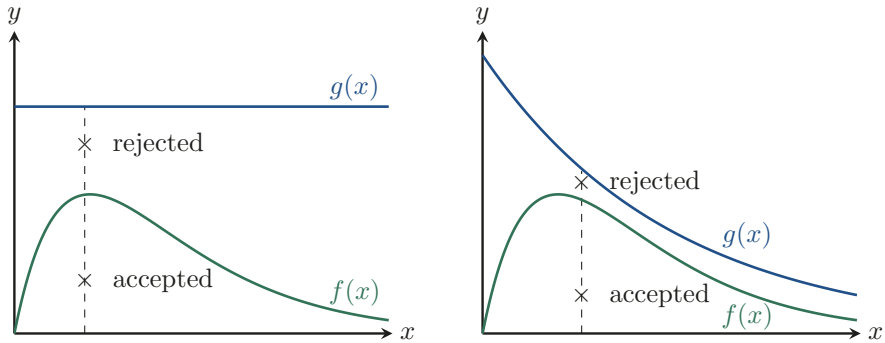

Figure 9: Illustrations of Monte Carlo accept/reject sampling from the probability distribution $f(x) = xe^{-x}$. Left: constant overestimate function $g(x)$, x is sampled uniformly. Right: Importance sampling with $g(x) = 2e^{-0.4x-1}$, x is sampled from $g(x)$ which (on average) decreases the number of reject samples.

Once we have picked an i we can sample x from $g_i(x)$ using the regular accept/reject method, except if we reject the sample we start over by picking a new i from I_i. This will give the correct statistics since

$$\int f(x)dx = \int \frac{f(x)}{g(x)} \sum_i g_i(x)dx = \sum_i I_i \int \frac{g_i(x)}{I_i} \frac{f(x)}{g(x)} dx. \tag{3.8}$$

3.2 Integration

Assuming for a momement that $f(x)$ is not a probability distribution but any smooth function that we want to integrate, i.e. we want to find

$$I = \int_{x_{\min}}^{x_{\max}} f(x)dx. \tag{3.9}$$

We then note that we already got the answer to this integral as a by-product from the accept/reject sampling. This since, when the total number of samples N tends to infinity, the ratio of the accepted samples to total samples times the overestimated area will give us the correct area, i.e.

$$I = [G(x_{\max}) - G(x_{\min})] \frac{N_{\text{accepted}}}{N} \tag{3.10}$$

with a corresponding error of (for the simple case of constant $g(x) = f_{\max}$)

$$\frac{\delta I}{I} = \frac{1}{\sqrt{N_{\text{accepted}}}}. \tag{3.11}$$

Table 1: Scaling of different numerical integration methods for N samples, in d dimensions.

Integration method	Error scaling
Monte Carlo	$1/N^{\frac{1}{2}}$
Trapezoid	$1/N^{\frac{2}{d}}$
Simpson	$1/N^{\frac{4}{d}}$

This way of using Monte Carlo to integrate is not the most efficient though, since we are only using the accept/reject statistics, and not full information of every $f(x)$ sampled. A more efficient way of approximating the integral is to use the full information for each $f(x)$. So, if we instead sample x uniformly between $x_{\min}$ and $x_{\max}$ it holds that (for N tending to infinity)

$$I = \frac{x_{\max} - x_{\min}}{N} \sum_{i=1}^{N} f(x_i). \tag{3.12}$$

The corresponding error is

$$\delta I = (x_{\max} - x_{\min}) \sqrt{\frac{\langle f^2 \rangle - \langle f \rangle^2}{N}}, \tag{3.13}$$

with

$$\langle f^n(x) \rangle = \frac{1}{N} \sum_{i=1}^{N} f^n(x_i). \tag{3.14}$$

Now, we have only looked at the simple case of solving for one integration variable, however the method above easily generalizes for multidimensional integrals. It is also there the true usefulness of Monte Carlo integration shows itself. If we compare the error above to the error of some of the other most common numerical integration techniques, shown in Table 1, we see that for one dimension, $d = 1$, Monte Carlo is not the most efficient. However, once we move up in dimensions we quickly get a big advantage of using Monte Carlo integration, as the scaling in error does not depend on dimension. There are numerous other factors which also makes Monte Carlo integration the preferred method, some of them being; it can deal with discontinuous functions and it gives a good first estimate from few sample points.

The method outlined above is the simplest case of Monte Carlo integration, and can be further refined. One way of doing this is to utilize the accept/reject overestimate function $g(x) \geq f(x)$, and noting that it can be viewed as a variable transformation,

$$I = \int f(x)dx = \int \frac{f(x)}{g(x)} g(x)dx = \int \frac{f(x)}{g(x)} dG(x) \approx \left\langle \frac{f}{g} \right\rangle \pm \sqrt{\frac{\langle f^2/g^2 \rangle - \langle f/g \rangle^2}{N}} \quad (3.15)$$

where the last term corresponds to the error. This way of integrating has the benefit of sampling more in regions where the integral is large, if one finds a good overestimate. We see from the error term that the error can be reduced significantly due to this.

Further improvements are available, some examples being the histogram method and stratified sampling, where in the former one splits up the sampling range of x into bins Δx, and then select which bin to sample from based on the maximum size of f in the bin, sampling more where f is larger. In the latter, one generalizes this even further and varies the sizes of the bins, so that each Δx_i is different, creating larger bins where df/dx is large, i.e. sampling more where f varies more.

3.3 Veto algorithm

The different sampling methods we have looked at so far have one thing in common, they lack *memory*. This presents a problem, since some processes we want to sample can require a certain memory of what has happened before. The process we mainly are thinking about here is the decay of particles, where a decay at time t can only occur if the particle has not decayed yet. We take radioactive decay as an example, and define $N(t)$ to be the probability that a single nucleus has not yet decayed at time t, also known as the *no-decay-probability*. We then have the probability that it will decay at time t defined as $P(t) = -dN/dt$. Naively, with no memory in time, we would assume that $P(t) = \lambda$ for some decay constant λ. This then leads to $N(t) = 1 - \lambda t$, which is clearly not correct, with a linear probability turning negative for large enough t. The correct way of treating this is is to assume that we have a probability of decay that goes like

$$P(t) = -\frac{dN}{dt} = f(t)N(t) \quad (3.16)$$

where $f(t)$ is the *instantaneous decay probability*. Solving for the no-decay-probability we get that

$$N(t) = e^{-\int_0^t f(t')dt'}, \quad (3.17)$$

which is also known as the *Sudakov-factor*. If $f(t)$ has a known invertible primitive function, and we assume that $\lim_{t\to\infty} F(t) = \infty$, i.e. it must decay at some point, we get that $N(t) \in [0, 1]$ and so for every random number $R \in [0, 1]$ there is a corresponding t such that $N(t) = R$, and t can be sampled as

$$t = F^{-1}(F(0) - \ln R). \quad (3.18)$$

As with the time-independent sampling we looked at before, we often encounter probability functions $f(t)$ with no known invertible primitive function. Once again, we can turn to accept/reject sampling by finding an overestimate $g(t) \geq f(t)$ with an invertible primitive function and sample from this instead. However, if we do this just as with the accept/reject sampling we described earlier, we will not get the correct statistics since we will then have used the Sudakov factor of the overestimate, i.e. we get the probability of decay

$$P(t) = \frac{f(t)}{g(t)} g(t) e^{-\int_0^t g(t')d't} = f(t) e^{-\int_0^t g(t')d't} \tag{3.19}$$

but we want

$$P(t) = f(t) e^{-\int_0^t f(t')d't}. \tag{3.20}$$

This leads us to what is called *the veto algorithm*, which is a slight, but important modification to the accept/reject sampling that corrects the Sudakov factor. It goes as outlined below.

(i) Find simple $g(t) \geq f(t)$ with known primitive function $G(t)$ and inverse primitive function $G^{-1}(t)$.

(ii) Set $t_0 = 0$.

(iii) Sample t from $g(t)N_g(t)$ (with t_0 as the lower integration bound in $N_g(t)$).

(iv) Sample new $R \in [0, 1]$ uniformly. If $R \leq f(t)/g(t)$ accept the value of t, otherwise reject it, but set $t_0 = t$ and cycle to (iii).

Hence, when we reject a value we move forward to the reject time and sample again from there, i.e. we *do not* restart at $t = 0$. This effectively gives our processes a memory. The veto algorithm can also easily be generalized for sampling both time and space for an instantaneous decay probability of the form $f(x, t)$, where x can be e.g. position or energy transfer.

Worth mentioning here is also multichannel decay, i.e. when we have a decay probability which goes as e.g. $f(t) = f_1(t) + f_2(t)$. The regular method outlined above still works, by finding an overestimate of the whole sum. However, we can also find an overestimate of each term in the sum separately, $g_1(t) \geq f_1(t)$ and $g_2(t) \geq f_2(t)$, and sample t_1 and t_2 independently from these over estimates. When both independent values t_1 and t_2 has been found and accepted, we then chooses the one that happens first in time. This method still preserves the correct decay rate, and is called the *winner-takes-all* method.

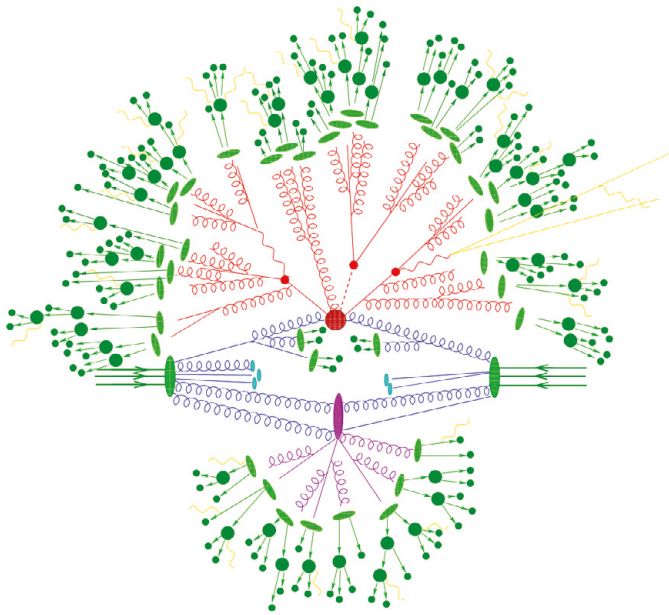

Figure 10: Illustration of the processes involved in the evolution of one event in the event generator SHERPA [41]. After an initial hard scattering (red circle) the resulting partons create parton cascades streaming out toward the detectors (red lines). At a later stage, they hadronize (green ellipses) and the hadrons can decay (green circles) until they finally free stream to the detectors. There are also multiple initial hard scattering events allowed (MPI, purple ellipse) which set in motion similar processes of parton cascades going to hadrons.

3.4 Event generators

A central tool which uses Monte Carlo methods in particle physics phenomenology are *event generators*. These are software which employ Monte Carlo methods to simulate a complete particle collision, called an *event*, evolving the system from the initial collision of the incoming particles (and even before through initial state radiation) up until the point where all the remnants of the initial collision have hadronized and free streamed to the detectors, using Monte Carlo methods. This is then repeated multiple times to produce statistical results which aim to be as similar to the actual data from from experiments as possible. From these results, one can extract predicted observable that are comparable to data from particle colliders, giving theorists the possibility to refine their theories by comparing theory to data, as well as experimentalists predictions of observables to look for in experiments. Experimentalist also use event generators to correct their data for detector effects. Event generators hence present the unique and essential opportunity for apples-to-apples comparisons between theory and data.

There exist many different event generators, some of which are more all-purpose and some

are designed for very specific processes. An example of some commonly used event generators for LHC physics are SHERPA [41], PYTHIA [40] and Herwig [42,43], and for heavy ion physics there is e.g. JEWEL [44], AMPT [45,46] and HIJING [47]. In Fig. 10 the structure of the evolution of an event is illustrated for the SHERPA event generator.

With the numerical toolset presented in this section at hand, we move on to look at the theory which can help us in resolving the contradiction of collective like behaviour in small collision systems; QCD effective kinetic theory.

4 QCD effective kinetic theory

In Ref. [1], P. Arnold, G. Moore and L. Yaffe (AMY) presented an effective kinetic theory for QCD at high temperatures. It is centered around the Boltzmann equation for a phase space density $f_s(\mathbf{x}, \mathbf{p}, t)$ of a particle of species s,

$$\left(\partial_t + \frac{\mathbf{p}}{p_0} \cdot \nabla_{\mathbf{x}}\right) f_s(\mathbf{x}, \mathbf{p}, t) = -C_s[f] \tag{4.1}$$

where $C_s[f]$ is the collision kernel, responsible for encoding the dynamics of the evolution of f_s. The Boltzmann equation is a general way of describing the statistical behaviour of an ensemble of particles that are out of equilibrium. It is commonly used in many areas of physics, e.g. when studying fluids and gases. We will use it to model the transport of partons in both small collision systems as well as heavy ion collisions since it is a valid description for out-of-equilibrium systems. To get a more intuitive view of the collision kernel that appear in the Boltzmann equation, we can first look at the phase space density for a species s, which can be related to the density of particles of that species in a small phase space-volume $d^6\xi = d^3\mathbf{x}d^3\mathbf{p}$,

$$\frac{dN_s}{d^6\xi} = \frac{\nu_s}{(2\pi)^3} f_s \tag{4.2}$$

where ν_s is the degeneracy of s. If there are no external forces acting on $d^6\xi$ it can be shown that [48]

$$\frac{d}{dt}\left(\frac{dN_s}{d^6\xi}\right) = \frac{\nu_s}{(2\pi)^3} C_s[f_s], \tag{4.3}$$

i.e. the collision kernel is related to the *total* time derivative of the phase space density. Hence the collision kernel C_s quantify the rate of change of the density of particles in $d^6\xi$, i.e. how many particles are entering and leaving $d^6\xi$ during some infinitesimal time interval dt.

In this section we will summarize the assumptions and derivations made to find which processes contribute to the collision kernel to leading order[9] and their corresponding collision

[9]Leading order in QCD running coupling $g(T)$ with T being temperature.

kernels. We end the section by looking at the simplified case of just allowing particles to scatter once in their evolution, and how collective flow is produced in this scenario.

4.1 Scales and relevant processes

In AMY kinetic theory a separation of scales is required, which gives us an ordering of different energy scales where each one relates to different dynamics of the system. We work in a unit system where we measure the temperature T in terms of energy (i.e. we have set the Boltzmann constant $k_{\mathrm{B}} = 1$). For large enough temperature T the QCD coupling $g(T)$ will be small, see e.g. Fig. 2 where we relate our temperature T to energy Q. Using this we define the hard scale of our theory to be T, while gT defines a softer scale. The theory is set up to describe typical particles in a thermal system, and the typical momentum is $\mathcal{O}(T)$, which we define as hard. Under this assumption the QCD plasma then consists of quarks and gluons as well-defined quasi-particles with typical momenta of order T. The soft scale is related to the collective motion of the individual particles, which in our case is through the thermal masses[10] of order $\mathcal{O}(gT)$, which we define as soft.

With these scale choices, we get an upper and lower bound for the energy transfer in elastic scattering, with the hard scale T setting the upper bound, and the soft scale gT setting the lower. Scattering below this scale is further softened by Debye screening and Landau damping, and can safely be neglected. The rate of elastic scatterings with energy transfer of $\mathcal{O}(T)$ is of order $\mathcal{O}(g^4T)$. This is often called large-angle scattering, since the direction of a particle can change by $\mathcal{O}(\mathbf{p}/T)$ for an energy transfer of $\mathbf{p}$. The rate of low energy transfer ($\mathcal{O}(gT)$) scatterings is of order $\mathcal{O}(g^2T)$, these are referred to as small-angle scatterings.

There are other processes that must be factored in as well, and those are collinear splitting and mergings, which occur at a rate of $\mathcal{O}(g^4T)$. These processes are not allowed to happen in a vacuum due to energy-momentum conservation. They are however allowed in a medium through soft interactions with other particles. This processes involves a propagator which is off-shell ($p_\mu p^\mu \neq 0$), and it is not instantaneous. The formation time for the process is of order $\mathcal{O}(g^2T)$, which is comparable to the soft elastic scattering rate. Hence, the particle can undergo multiple soft scatterings during the formation time, making it a $N + 1 \leftrightarrow N + 2$ process. The additional soft scatterings cannot be resolved individually and instead act coherently, which gives rise to a QCD version of what is known as the Landau-Pomeranchuk-Migdal (LPM) effect. We will refer to these processes as "$1 \leftrightarrow 2$" processes, or collinear splitting/merging.

Hence, our system consists of hard partons propagating through the medium as nearly free and nearly massless particles, since thermal masses are $\mathcal{O}(gT)$ and the small-angle scattering rate is $\mathcal{O}(g^2T)$. The rate of large-angle scattering as well as collinear splitting and merging is $\mathcal{O}(g^4T)$. These allowed processes and rates are illustrated in Fig. 11.

The corresponding Boltzmann equations takes the form of

[10] These are effective masses that appear as corrections to the dispersion relation of the particles propagating the medium, $\epsilon(\mathbf{p}) = \sqrt{|\mathbf{p}|^2 + m^2_{\mathrm{effective}}}$.

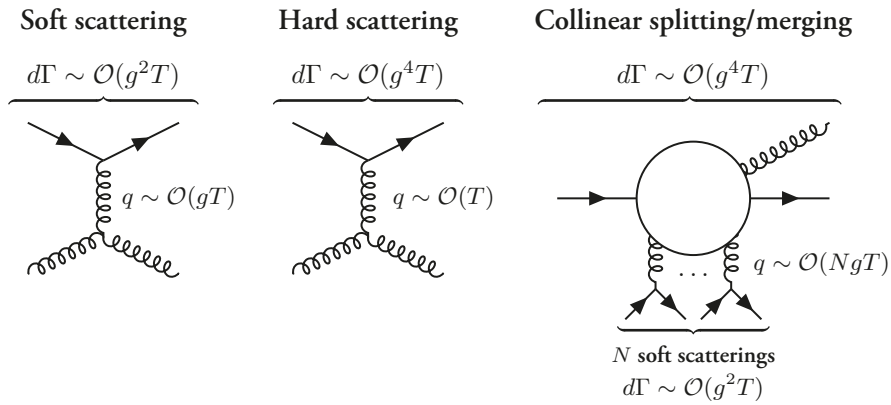

Figure 11: Examples of the three different processes that contribute to leading order in AMY QCD effective kinetic theory. The scattering/splitting/merging rates are denoted $d\Gamma$, and energy transfer of the interaction is denoted as q. Left and center: elastic $2 \leftrightarrow 2$ with low and high (soft and hard) energy transfer respectively. Right: "$1 \leftrightarrow 2$" processes, i.e. splitting or merging, where the formation time for the processes allows for N soft scatterings to occur with the medium.

$$\left(\partial_t + \frac{\mathbf{p}}{p_0} \cdot \nabla_{\mathbf{x}}\right) f_s(\mathbf{x}, \mathbf{p}, t) = -C_s^{2\leftrightarrow 2}[f] - C_s^{\text{"}1\leftrightarrow 2\text{"}}[f] \tag{4.4}$$

where the two different kinds of processes are separated into two collision kernels, with $2 \leftrightarrow 2$ corresponding to elastic scattering and "$1 \leftrightarrow 2$" corresponding to inelastic splitting and merging.

The effective kinetic theory of AMY is valid for equilibrium, near equilibrium and out-of-equilibrium systems, under certain conditions. The full list of conditions can be found in Ref. [1], though two of the key conditions for remaining valid in non-equilibrium systems are centered around the effective mass $m_{\text{effective}}$ which we will define in the next section. The first condition is that we have a clear separation of scales, meaning

$$\frac{m_{\text{effective}}}{p_{\text{hard}}} \lesssim \mathcal{O}(g^2), \tag{4.5}$$

and the second condition is that the effective mass must be large compared to the small-angle scattering rate, which is of order $\mathcal{O}(g^2T)$.

4.2 Elastic scattering

The dynamics of the elastic scattering processes are encoded in the collision kernel

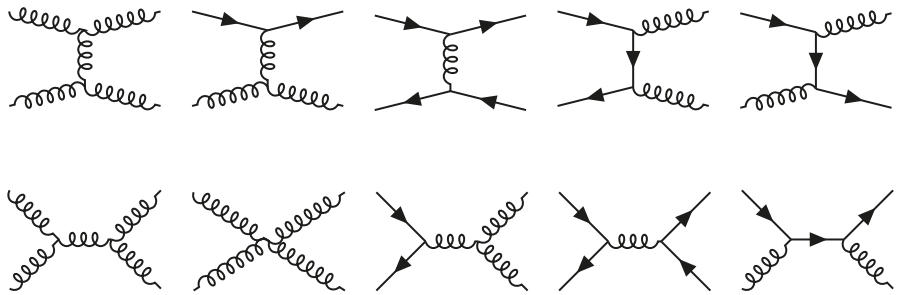

Figure 12: Allowed $2 \leftrightarrow 2$ elastic scattering processes in AMY QCD effective kinetic theory. For each diagram containing quarks there also exists a corresponding diagram with $q \leftrightarrow \bar{q}$.

$$C_a^{2\leftrightarrow 2}[f(\mathbf{p})] = \frac{1}{4|\mathbf{p}|}\sum_{bcd}\int_{\mathbf{kp'k'}} \nu_b |\mathcal{M}_{cd}^{ab}|^2 (2\pi)^4 \delta^{(4)}(P+K-P'-K') \\ \times \{f_a(\mathbf{p}) f_b(\mathbf{k})[1 \pm f_c(\mathbf{p}')][1 \pm f_d(\mathbf{k}')] - f_c(\mathbf{p}') f_d(\mathbf{k}')[1 \pm f_a(\mathbf{p})][1 \pm f_b(\mathbf{k})]\}\,. \quad (4.6)$$

Here, $|\mathcal{M}_{cd}^{ab}|$ is the matrix element for a process $ab \leftrightarrow cd$. The first term in the curly brackets corresponds to the *loss term*, i.e. particles *leaving* some infinitesimal volume in phase space centered around $\mathbf{p}$. The second term in the curly brackets corresponds to the *gain term*, i.e. particles entering this volume around $\mathbf{p}$. The terms in the square brackets are Bose-enhancement and Pauli blocking, for $+$ (gluons) and $-$ (fermions) respectively. The integral notation used is

$$\int_{\mathbf{p}} \cdots = \int \frac{d^3\mathbf{p}}{2|\mathbf{p}|(2\pi)^3}. \quad (4.7)$$

The factor ν_b is the degeneracy of the state b in terms of spin and color, so $\nu_{q/\bar{q}} = 6$ and $\nu_g = 16$. The difference of a missing $1/\nu_a$ and one new factor ν_b compared to [1] is due to the matrix elements presented there being summed over the spin and color of both initial and final state, while the matrix element shown here is averaged over the incoming states, and summed over the outgoing.

The allowed processes which contribute to the dynamics are shown in Fig. 12, and their corresponding matrix elements in Table 2. As can be seen there, many of them are divergent for small Mandelstamm t and u. This is remedied by the medium-dependent effects that appear in thermal field theory, through the effective masses of gluons and fermions, which act to regulate the divergent matrix elements.

The *effective* (or *screening*) *mass*, m_s, for a particle of species s, represents the medium screening effects. It contributes, through regulating the divergent matrix element, in a highly non-trivial way to the evolution of the phase space densities. The (position averaged)

Table 2: Matrix elements for the allowed elastic scattering processes [1,49]. The notation q_1 and q_2 represent quarks of distinct flavours. The numerical factors d_F and d_A are the dimensions of the fundamental and adjoint representation of the fermions and gauge bosons reprectively. The factors C_F and C_A are the corresponding quadratic Casimirs. For QCD it holds that $d_F = C_A = 3$, $C_F = 4/3$ and $d_A = 8$ (corresponding to the symmetry SU(3)).

$ab \leftrightarrow cd$	$\lvert\mathcal{M}_{cd}^{ab}\rvert^2/g^4$
$q_1q_2 \leftrightarrow q_1q_2$ $q_1\bar{q}_2 \leftrightarrow q_1\bar{q}_2$ $\bar{q}_1q_2 \leftrightarrow \bar{q}_1q_2$ $\bar{q}_1\bar{q}_2 \leftrightarrow \bar{q}_1\bar{q}_2$	$8\frac{d_F^2C_F^2}{d_A}\left(\frac{s^2+u^2}{t^2}\right)$
$q_1q_1 \leftrightarrow q_1q_1$ $\bar{q}_1\bar{q}_1 \leftrightarrow \bar{q}_1\bar{q}_1$	$8\frac{d_F^2C_F^2}{d_A}\left(\frac{s^2+u^2}{t^2}+\frac{s^2+t^2}{u^2}\right)+16d_FC_F\left(C_f-\frac{C_A}{2}\right)\frac{s^2}{tu}$
$q_1\bar{q}_1 \leftrightarrow q_1\bar{q}_1$	$8\frac{d_F^2C_F^2}{d_A}\left(\frac{s^2+u^2}{t^2}+\frac{t^2+u^2}{s^2}\right)+16d_FC_F\left(C_f-\frac{C_A}{2}\right)\frac{u^2}{st}$
$q_1\bar{q}_1 \leftrightarrow q_2\bar{q}_2$	$8\frac{d_F^2C_F^2}{d_A}\left(\frac{t^2+u^2}{s^2}\right)$
$q_1\bar{q}_1 \leftrightarrow gg$	$8d_FC_F^2\left(\frac{u}{s}+\frac{t}{u}\right)-8d_FC_FC_A\left(\frac{t^2+u^2}{s^2}\right)$
$q_1g \leftrightarrow q_1g$ $\bar{q}_1g \leftrightarrow \bar{q}_1g$	$-8d_FC_F^2\left(\frac{u}{s}+\frac{s}{u}\right)+8d_FC_FC_A\left(\frac{s^2+u^2}{t^2}\right)$
$gg \leftrightarrow gg$	$16d_AC_A^2\left(3-\frac{su}{t^2}-\frac{st}{u^2}-\frac{tu}{s^2}\right)$

definition of the effective mass is given as

$$m_g^2 = \sum_s 2\nu_s \frac{g^2C_s}{d_A}\int_V \frac{d^3\mathbf{x}}{V}\int \frac{d^3\mathbf{p}}{2|\mathbf{p}|(2\pi)^3} f_s(\mathbf{p},\mathbf{x}) \tag{4.8}$$

for gluons, and for a fermion of species s

$$m_{q(s)/\bar{q}(s)}^2 = 2g^2C_F\int_V \frac{d^3\mathbf{x}}{V}\int \frac{d^3\mathbf{p}}{2|\mathbf{p}|(2\pi)^3}\left[2f_g(\mathbf{p},\mathbf{x})+f_s(\mathbf{p},\mathbf{x})+f_{\bar{s}}(\mathbf{p},\mathbf{x})\right] \tag{4.9}$$

where $C_A = 3$ and $C_F = 4/3$ are the quadratic Casimirs and $d_A = 8$ the dimension of the adjoint representation of the gluon. Since $d^3\mathbf{p}/|\mathbf{p}|$ is a Lorentz invariant measure, and f is Lorentz scalar [50], it follows that the effective masses are Lorentz scalars.

For hard scattering the screening effects are negligible. For soft scattering one can effectively use the screening masses defined above to regulate the divergent t and u-channels in the

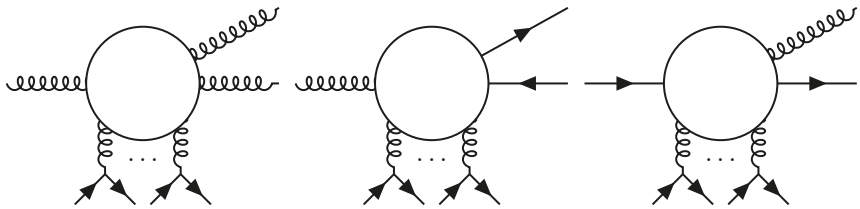

Figure 13: The three types of possible splittings and mergings in AMY kinetic theory; $g \leftrightarrow gg$, $g \leftrightarrow q\bar{q}$ and $q \leftrightarrow gq$ (where $\bar{q} \leftrightarrow g\bar{q}$ is also possible) from left to right.

matrix elements as e.g.

$$\frac{1}{t^2} \to \frac{1}{(t-\zeta_s m_s^2)^2} \quad \text{and} \quad \frac{1}{u^2} \to \frac{1}{(u-\zeta_s m_s^2)^2}, \tag{4.10}$$

where the species s depends on whether the relevant process exchanges a virtual gluon of fermion. The factor ζ_s is a numerical factor which depends on the choice of regularization[11].

4.3 Inelastic splitting and merging

The collision kernel for the splitting and merging is constructed in a similar way as the one for elastic scattering. However, only exact collinear splittings and mergings are kinematically allowed for massless particles (and almost collinear splittings and mergings for particles with small masses) in order to preserve both energy and momentum. Hence, we can integrate over the small transverse momentum of the process, giving us the expression

$$\begin{aligned} C_a^{\text{“}1\leftrightarrow 2\text{”}}[f] =& \frac{(2\pi)^3}{2|\mathbf{p}|^2\nu_a}\sum_{b,c}\int_0^\infty dp'\,dk'\delta(p-p'-k')\gamma^a_{bc}(\mathbf{p};p'\hat{\mathbf{p}},k'\hat{\mathbf{p}}) \\ &\times\Big\{f_a(\mathbf{p})[1\pm f_b(p'\hat{\mathbf{p}})][1\pm f_c(k'\hat{\mathbf{p}})] - f_b(p'\hat{\mathbf{p}})f_c(k'\hat{\mathbf{p}})[1\pm f_a(\mathbf{p})]\Big\} \\ &+\frac{(2\pi)^3}{|\mathbf{p}|^2\nu_a}\sum_{b,c}\int_0^\infty dk\,dp'\delta(p+k-p')\gamma^a_{bc}(p'\hat{\mathbf{p}};\mathbf{p},k\hat{\mathbf{p}}) \\ &\times\Big\{f_a(\mathbf{p})f_b(k\hat{\mathbf{p}})[1\pm f_c(p'\hat{\mathbf{p}})] - f_c(p'\hat{\mathbf{p}})[1\pm f_a(\mathbf{p})][1\pm f_b(k\hat{\mathbf{p}})]\Big\}. \end{aligned} \tag{4.11}$$

Here, γ^a_{bc} represent the parameterized splitting/merging rate for a process $a \leftrightarrow bc$. In Paper II we construct a simple parametrization for $\gamma = \gamma(p, x, m_g^2, T_*)$, which is shown to depend only on the total incoming (for splitting, outgoing for merging) amplitude of the momentum p, the energy fraction x, the effective mass of gluons m_g and the effective

[11]The factors ζ_s should contain a conversion factor between asymptotic effective mass and screening mass, as well as a scaling factor that ensures that the modified matrix elements reproduce, to leading order, the hard thermal loop results for drag and momentum broadening, see e.g. Refs. [51–53].

temperature T_*. This temperature is the effective temperature at which an equilibrium system would have the same soft elastic scattering rate as the system under consideration. The definition of T_*, averaged over a spatial volume V, is given by

$$T_* = \frac{\frac{1}{2}g^2 \sum_s \frac{\nu_s C_s}{d_A} \frac{1}{V} \int d^3\mathbf{x} \int \frac{d^3\mathbf{p}}{(2\pi)^3} f_s(p)[1 + f_s(p)]}{g^2 \sum_s \frac{\nu_s C_s}{d_A} \frac{1}{V} \int d^3\mathbf{x} \int \frac{d^3\mathbf{p}}{(2\pi)^3} f_s(p)/p} \tag{4.12}$$

where we note that the denominator is equal to m_g^2. The numerator of T_* is not a Lorentz scalar, and is defined in the fluid rest frame.

As mentioned in Section 4.1 the splitting and merging processes do not happen instantaneously, they have a formation time in which multiple soft interactions with the medium can occur. This formation time is given by

$$t_{\text{form}} = \frac{p}{m_g^2} \left[1 + \frac{g^4 T_* p}{m_g^2}\right]^{-\frac{1}{2}}. \tag{4.13}$$

We now end the brief overview of the underlying theory of AMY kinetic theory, and move on to look at one specific application of it.

4.4 Single-hit approximation

In Paper I we investigate energy flow response to initial geometry deformations, when the system is evolving according to AMY kinetic theory. We do this under the simplifying assumption that particles only experience at most one scattering, and we look at a purely gluonic system. In this section we, very briefly, outline the procedure and review some key results. The full details of the derivations, as well as all the results, are found in Paper I.

We start by first considering the free-streaming solution (i.e. the solution to the Boltzmann equations where the collision kernel $C[f] = 0$), which can be written entirely in terms of the initial distribution $f^{(0)}$ given at time t_0 using the *co-moving coordinates* [54],

$$p_z \to \tilde{p}_z = \frac{t}{t_0} p_z, \tag{4.14}$$

$$\mathbf{p}_\perp \to \mathbf{p}_\perp \tag{4.15}$$

and

$$\mathbf{x}_\perp \to \tilde{\mathbf{x}}_\perp = \mathbf{x}_\perp - \frac{\mathbf{p}_\perp}{p_\perp^2} t \left(\sqrt{p_\perp^2 + p_z^2} - \frac{t_0}{t} \sqrt{p_\perp^2 + p_z^2 \frac{t^2}{t_0^2}} \right). \tag{4.16}$$

With these coordinates, the free streaming distribution for any time t becomes

$$f^{(0)}(t, \mathbf{x}_\perp; \mathbf{p}_\perp, p_z) = f^{(0)}(t_0, \tilde{\mathbf{x}}_\perp; \mathbf{p}_\perp, \tilde{p}_z). \tag{4.17}$$

We define the co-moving distribution function

$$\tilde{f}(t, \tilde{\mathbf{x}}_\perp; \mathbf{p}_\perp, \tilde{p}_z) = f(t, \mathbf{x}_\perp; \mathbf{p}_\perp, p_z) \tag{4.18}$$

which then reduces the Boltzmann equation to an ordinary differential equation in time t,

$$\partial_t \tilde{f}(t, \tilde{\mathbf{x}}_\perp; \mathbf{p}_\perp, \tilde{p}_z) = -\tilde{C}[\tilde{f}](t, \tilde{\mathbf{x}}_\perp; \mathbf{p}_\perp, \tilde{p}_z). \tag{4.19}$$

Next we linearize the solution to the co-moving Boltzmann equations *in the number of scatterings* $\tilde{f} = \tilde{f}^{(0)} + \tilde{f}^{(1)} + \ldots$, where the free streaming and the single-scattering distributions evolve according to

$$\partial_t \tilde{f}^{(0)} = 0, \tag{4.20}$$

$$\partial_t \tilde{f}^{(1)} = -\tilde{C}[\tilde{f}^{(0)}]. \tag{4.21}$$

This is what is known as *the single-hit approximation*, and the first correction to the distribution can be obtained directly by integration

$$\tilde{f}^{(1)}(t) = -\int_{t_0}^{t} dt' \tilde{C}[\tilde{f}^{(0)}](t'), \tag{4.22}$$

where by definition the initial condition for the perturbation is $\tilde{f}^{(1)}(t_0) = 0$, since no particle has had time to undergo any scatterings.

We also linearize in small azmiuthal perturbations in position space, δf, of the otherwise symmetric background, i.e.

$$f^{(0)}(t_0, \mathbf{x}_\perp; \mathbf{p}_\perp, p_z) = \bar{f}(t_0, x_\perp; \mathbf{p}, p_z) + \delta f(t_0, x_\perp, \phi_{\mathbf{x}}; \mathbf{p}, \mathbf{x}_\perp). \tag{4.23}$$

This further simplifies our calculations, and has the added benefit that it allows us to clearly study the *escape mechanism*, as illustrated in Fig. 14. Taking an elliptic deformation as example: when particles are initialized isotropically in momentum but anisotropically in space, with an excess of particles along the x-axis, the flow of particles will after some time create an excess of particles with momentum pointing along the x-axis at the origin. The kinetic theory of AMY acts to locally equilibrate the system, and so at the origin momentum in the x-direction will be removed and momentum along the y-direction will be created due to elastic scattering. Since we started out globally isotropic in momentum (as seen from far away, at $r \to \infty$), we have now created a globally anisotropic system with more momentum flow in along the y-axis. This is causing a contribution to positive elliptic flow v_2, and is what is known as the escape mechanism.

We use the simplifying assumptions above in combination with Color Glass Condensate-like initial conditions [55, 56] to study the energy flow coefficients in Eq. (2.5); v_n. We

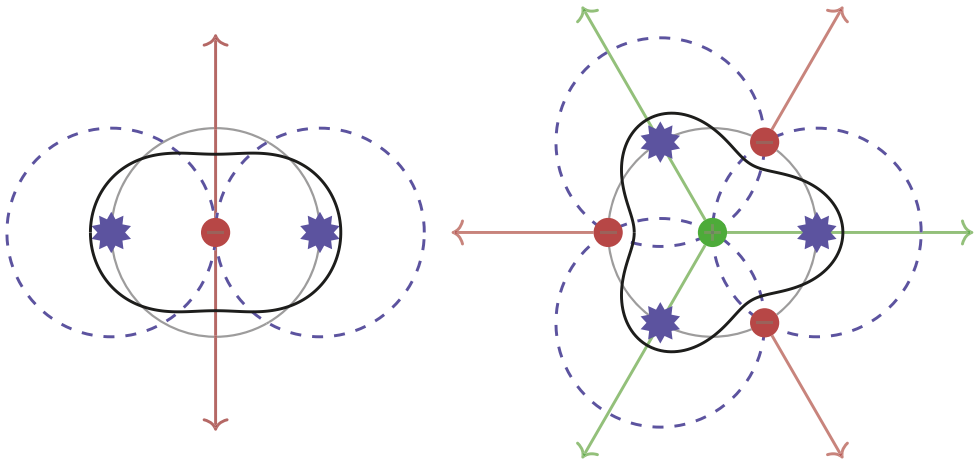

Figure 14: Illustration of the production of elliptic and triangular flow due to initial geometrical deformations. We model the initial spatial anisotropy as hotspots (blue stars) with an excess of particles initialed isotropic in momentum there. After some time, the particles from the hotspots will have reached the origin (dashed blue lines), creating an excess of horizontal movers there. The local isotropization of AMY kinetic theory then removes horizontal movers and creates vertical movers. This creates a momentum anisotropy which is anti-aligned with the initial spatial anisotropy, which corresponds to the production of collective flow. This holds for both v_2 (left) and v_3 (right). For v_2, and as the particles from the hotspots move further away they will continue to intersect along the axis anti-aligned with the initial spatial anisotropy. For v_3 the intersections will be in two directions though, both aligned and anti-aligned with the initial spatial anisotropy. Since the local isotropization occurs in the local rest frame, it means that one of the intersection directions will produce negative triangular flow (since the rest frame is moving away from the origin), and the other positive triangular flow.

start by deriving an analytic expression for these coefficients which we can solve numerically. We then use this result to study the flow production of elliptic and triangular flow, which are shown to correspond to the arguments of the escape mechanism. Next we use the conformal symmetry of the system to express the flow coefficients through a scaling formula,

$$\frac{v_n}{\epsilon_n} = \hat{R}\left[\hat{v}_n^{\text{cl.}}(\hat{m}_g^2) + \hat{A}\hat{v}_n^{\text{b.e.}}(\hat{m}_g^2)\right] \tag{4.24}$$

where ϵ_n is the initial eccentricity. The variable $\hat{A}$ is a scaled version of the occupancy, i.e. the number of particles allowed in a given state at some energy, $\hat{R}$ a scaled version of the system size in units of the mean free path and $\hat{m}_g^2$ a scaled version of the screening mass. All of these variables are expressed in terms of other initial parameters of the theory, and

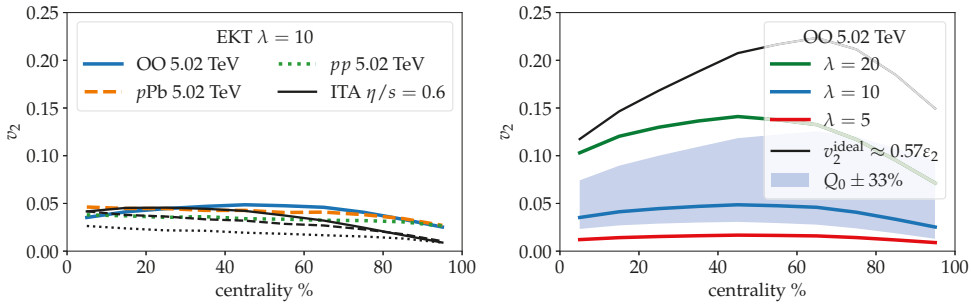

Figure 15: Elliptic flow for small collision systems using Color Glass Condensate-like initial conditions, as functions of centrality. The results are extracted from the scaling formula derived in Paper I. The left figure shows collective flow for different small collision systems at fixed λ, while the right figure shows collective flow for $\mathrm{O}+\mathrm{O}$ for different lambda, and varying initial characteristic energy scale (blue band). All details about the figures can be found in Paper I.

are explained in detail in Paper I. The functions $\hat{v}_n^{\text{cl.}}$ and $\hat{v}_n^{\text{b.e.}}$ cannot be extracted through scaling behaviour alone due to the screening mass acting in them in a non-trivial way, and so we find them numerically. This gives us a pocket-formula for the collective flow, which we use for a proof-of-principle study to predict the elliptic flow for $\mathrm{p}+\mathrm{p}$, $\mathrm{p}+\mathrm{Pb}$ and $\mathrm{O}+\mathrm{O}$ collisions. These predictions turn out to be correct in order of magnitude, see Fig. 15.

We also revisit the single-hit approach in Paper IV, using a more numerical approach to extract v_2, described in more detail in the next section.

We have now outlined all the relevant theory needed to present the main work of this thesis where we tie it all together; the Monte Carlo event generator Alpaca.

5 ALPACA

In this thesis we started out by showing a possible argument for *why* one would like to do physics. The same argument also implied that if one wants to do physics, one should be concerned with any emergent contradiction within the theory. This gave us a possible answer to *what to do* in physics, as we highlighted a contradiction within the field of heavy ion physics. We then reviewed some theoretical background needed to understand this contradiction, of measured signs of collective behaviour in small collision systems. This then allowed us to move on to answer two questions. The first of those were *what theory* could solve this; with our answer being the QCD effective kinetic theory of AMY. The second was *what methods* could we use to extract sensible predictions from this theory which allows for apple-to-apple comparison with available data; with our answer being Monte Carlo methods implemented in an event generator. It is now time to put it all in place and discuss *how* we have actually implemented this.

In this section we give an overview of the work presented in Paper II-IV, where we introduce the event generator ALPACA (AMY Lorentz invariant PArton CAscade). This is the main work of my PhD studies, and my attempt to contribute to resolving the contradiction of signs of collective behaviour in small collision systems.

ALPACA is a parton cascade which solves the Boltzmann equation of the AMY effective kinetic theory indirectly by, in a Lorentz invariant way, evolving a parton ensemble with corresponding phase space density $f_s(p)$ according to the AMY collision kernels. It is constructed as a module to the multi-purpose event generator SHERPA. As introduced in Section 4, three types of dynamic processes are needed in order to capture the dynamics of these kernels: elastic scattering, quasi-collinear merging and quasi-collinear splitting. Each of the processes also requires two or three of the dynamic quantities $m^2_{g/q}$, $f(p)$ and T_*.

In this section we will give a rough outline of the methods used to implement all of the above and summarize some key results, all details can be found in Paper II-IV. We start by discussing the concept of Lorentz invariance, and how we implement this.

5.1 Lorentz invariance

Quantities which do not depend on which inertial frame we choose to calculate/measure them in are called Lorentz scalars, and models which evolve in the same way independent of which frame we view them in are called Lorentz invariant models. The no-interaction theorem [57] states that N particles moving in a $6N$ dimensional phase space cannot interact if Lorentz invariance is required. It is however possible to circumvented this theorem by regarding the particles as moving in a $8N$ dimensional phase space, see Ref. [58], i.e. formulating the theory in terms of four-positions and four-momenta of the particles.

The position x^μ and momentum p^μ can be parameterised by an evolution parameter τ that is a Lorentz scalar. We get the equations of motions by following the approach of Ref. [59]. In short, we assume a simplified Hamiltonian, in which there are only binary interactions of particles taking place at discrete points in τ. Hence, our particles move as free pointlike particles between binary interactions. We will also neglect all particle masses as thermal masses are parametrically small compared to the momenta, and treat our particles as massless.

We also utilize the Lorentz invariant distance

$$d_{ij}^2 = -\left(x^2 - \frac{(x_\mu p^\mu)^2}{p^2}\right) \tag{5.1}$$

where $x = x_i - x_j$ is the relative four-distance between the particles, and $p = p_i + p_j$. Minimizing this in combination with the equations of motions derived from the Hamiltonian allows us to find a Lorentz invariant closest approach between particle pairs, with a corresponding $\tau_{\text{c.a.}}$. Hence, we can order our events in a frame independent way using $\tau_{\text{c.a.}}$, which we will look closer at how to do in the next subsection.

5.2 Scattering, splitting and merging

To implement a framework which dynamically evolves a discrete parton ensamble according to the collision kernels of AMY kinetic theory, we will utilize the Lorentz invariant setup described in the previous subsection, in combination with a selection of the Monte Carlo methods introduced in Section 3. We will evolve our system in the Lorentz scalar τ, and for each τ we will evaluate at which τ' the next scatter/split/merge will occur.

The main idea for evaluating the elastic scattering is that we at the current τ of the simulation find $\tau_{\text{c.a.}}$ in terms of d_{ij} for each particle pair i and j, giving us a corresponding $\tau_{ij,\text{scatter}} > \tau$. A scattering is then decided to occur if the invariant distance at closest approach falls within the corresponding $2 \leftrightarrow 2$ cross-section, i.e. if $d_{ij} \leq \sqrt{\sigma_{ij}/\pi}$. Hence, we would then like to calculate the cross-section of an elastic scattering, Eqs. (1.5) and (1.3). In the cross-section we use the matrix elements of the $2 \leftrightarrow 2$ collision kernel, as shown in Table 2. However, the cross-section will depend on local quantities such as $m^2_{g/q}(\tau_{ij,\text{scatter}})$ as well as the outgoing kinematics, e.g. $f(\tau_{ij,\text{scatter}}, p')$. These quantities can be approximated by letting the system free stream from our τ of evaluation to $\tau_{ij,\text{scatter}}$, however, other events may occur at some τ' such that $\tau < \tau' < \tau_{ij,\text{scatter}}$. Such events can cause a change in our approximated dynamic quantities, and so our probability for elastic scattering between partons i and j would not be correct.

This is solved by accept/reject Monte Carlo. At the current τ of the simulation, we find the closest approach for all particle pairs i and j, and then we find overestimates of the actual cross-section, $\sigma^{\text{o.e.}}_{ij} \geq \sigma_{ij}$. If the distance between the particles at the closest approach falls within the cross-section, i.e. $d_{ij} \leq \sqrt{\sigma^{\text{o.e.}}_{ij}/\pi}$, we keep $\tau_{ij,\text{scatter}}$ as a potential scattering. We then let the system evolve in τ, and when we reach $\tau_{ij,\text{scatter}}$ of the potential scattering we calculate the real cross-section σ_{ij}. We then accept the scattering with a probability of $\sigma_{ij}/\sigma^{\text{o.e.}}_{ij}$. This gives us the correct scattering statistics. We will discuss how to locally extract the dynamic quantities $m^2_{g/q}$ and f in the next subsection.

For mergings we proceed in a similar way as with the elastic scattering, we calculate an overestimate of the cross-section, and accept/reject based on the real value at the τ of closest approach. There are certain differences that factor in here though. The main difference is the fact that we cannot kinematically have a process $ab \to c$ and preserve both energy and momentum, if it is not exactly collinear. Since we are dealing with a discrete ensemble, we will not have particles moving exactly collinearly. We resolve this by allowing for a small relative transverse momentum between the incoming partons, $k_\perp$, assuming that the probability distribution for $k_\perp$ should go as $dk^2_\perp/k^2_\perp$. This is enforced in the cross-section. We also introduce a *recoil parton*, which we pick to be any particle close to the merging. This recoil parton will effectively act as the medium and absorb any recoil due to the small $k_\perp$ so that all partons stay on-shell. We also need to known the effective temperature T_*, which we describe how to extract in the next subsection. Lastly, we assign a formation time following Eq. (4.13) to the merging pair such that no other interaction can happen during this time interval.

For the splitting it works quite differentl. Since we do not have a parton pair, we can-

not look at the closest approach any more. Here, we instead use the Veto Algorithm as described in Section 3.3. We extract the instantaneous splitting probability, and its overestimate, from the splitting term of the "$1 \leftrightarrow 2$" collision kernel. As for the merging, we allow for a small $k_\perp$ which we sample from $dk_\perp^2/k_\perp^2$ when calculating the outgoing kinematics. Here also a close by recoil parton is involved to absorb the recoil. As with the merging, a formation time is also assigned.

5.3 Dynamic quantities

For each process described in the previous subsection we extract the dynamic quantities $m_{g/q}^2$, T_* and f locally as follows.

For the screening masses $m_{g/q}^2$ we assume that the particles are pointlike allowing us to express the phase space density as

$$\frac{dN_a}{d^3\mathbf{x}d^3\mathbf{p}} = \frac{\nu_a}{(2\pi)^3} f_a(\mathbf{x},\mathbf{p}) = \sum_i \delta^3(\mathbf{x}_i - \mathbf{x})\delta^3(\mathbf{p}_i - \mathbf{p}) \tag{5.2}$$

which turns the expressions for the screening masses, Eqs. (4.8) and (4.9) to sums over the partons in the event. We then include the N_{inc} closest (in space) particles to contribute to the sum, and normalize over the spherical volume centered at $\mathbf{x}$, created by the particle furthest away out of the N_{inc} included particles. The parameter N_{inc} has to be chosen, and is looked at in detail in Paper II.

The effective temperature T_* is calculated in a similar way, though the pointlike approximation does not work due to the squared phase space density (f^2) in Eq. (4.12). This would give us a square Dirac delta term, $(\delta^{(3)}(\mathbf{x}_i - \mathbf{x})\delta^{(3)}(\mathbf{p}_i - \mathbf{p}))^2$ which is not well defined. We instead approximate the partons as Gaussians,

$$f_a(\mathbf{x},\mathbf{p}) = \frac{(2\pi)^3}{\nu_a} \sum_i \frac{e^{-\frac{(\mathbf{x}_i-\mathbf{x})^2}{2\sigma_{i,\mathbf{x}}^2}} e^{-\frac{(\mathbf{p}_i-\mathbf{p})^2}{2\sigma_{i,\mathbf{p}}^2}}}{(2\pi\sigma_{i,\mathbf{x}}\sigma_{i,\mathbf{p}})^3} \tag{5.3}$$

which again allows us to include the N_{inc} closest particles that each contribute to the sum through individual terms, as well as the mixed terms from f^2.

Lastly, for the phase space density $f(\mathbf{x},\mathbf{p})$ we once again approximate the partons as pointlike and simply count how many partons N exists in a volume in phase space $V = V_\mathbf{x} V_\mathbf{p}$ where $V_\mathbf{x}$ is a sphere centered at $\mathbf{x}$ and $V_\mathbf{p}$ is a spherical shell around the origin containing the magnitude of the momentum, $|\mathbf{p}|$. This then gives us the phase space density as

$$f_a(\mathbf{x},\mathbf{p}) = \frac{(2\pi)^3}{\nu_a} \frac{N_{\text{inc}}}{V}. \tag{5.4}$$

We also set an upper bound for the extracted phase space density such that $f_a(\mathbf{x},\mathbf{p}) \leq T_*/p$, since the underlying theory is not valid for $f(p) > T_*/p$. This implementation is for

isotropic distributions, i.e. $f(\mathbf{x}, \mathbf{p}) = f(\mathbf{x}, p)$, since we are mainly interested in that to begin with. It is, however, easily generalizable to anisotropic distributions by instead of a spherical shell in momentum space using a sphere centered at $\mathbf{p}$.

This (briefly) summarizes the main parts of ALPACA responsible for the evolution of the parton ensemble according to the AMY kinetic theory. There are numerous details left out in this overview, which all are described in detail in Paper II. We now move on to look at the validation of the framework.

5.4 Thermal equilibrium

To evaluate the validity of our implementation, we start by looking at the case of an infinite fluid/medium in thermal equilibrium. This provides us with a simple setting where many quantities can be found analytically, such as e.g. the elastic scattering rate and screening masses. We look at both the classical case of a thermal equilibrium distribution using the Boltzmann distribution,

$$f_{g/q/\bar{q},\text{initial}}(p) = f_{\text{C}}(p) = e^{-p/T} \tag{5.5}$$

as well as the quantum case of Bose-Einstein and Dirac-Fermi distributions,

$$f_{g,\text{initial}}(p) = f_{\text{BE}}(p) = \frac{1}{e^{p/T} - 1} \quad \text{and} \quad f_{q/\bar{q},\text{initial}}(p) = f_{\text{FD}}(p) = \frac{1}{e^{p/T} + 1}. \tag{5.6}$$

Note that we use a unit system where we measure temperature T in units of energy (GeV), i.e. we have fixed the Boltzmann constant $k_{\text{B}} = 1$. To turn our discrete ensemble to an infinitely extended homogeneous system we initialize our system in a box with periodic boundary conditions. This introduced some complications due to our Lorentz invariant way of finding the closest approach, as it depends on momentum. If we were looking for the closest approach in terms of regular Euclidian distance, we would only have to consider the distance between a particle i and j, as well as the 26 copies of j in the closest surrounding copies of the original box. Now however, we have to consider all possible copies infinitely far away. We implement a solution to this problem, but it is rather technical and so we leave it for Paper II.

With our system setup in thermal equilibrium, we first investigate all the parts of our implementation piece wise and compare to analytical and simpler numerical results. We find that they all give the expected correct behaviour within errors. We then end the validation by putting everything together and run events over long times with all processes extracted dynamically (cross sections, γ, effective mass and temperature, phase space density), initializing with both quarks and gluons. The results are as expected; up to minor fluctuations and small shifts in particle number and average energy, the system stays in thermal equilibrium. A selection of the results from the long run can be seen in Fig. 16 and 17. In the former we see the distribution at the end of the run, and in the latter we see screening mass and effective temperature converging to the correct value. This shows that our parton cascade faithfully reproduces the dynamic of the AMY kinetic theory collision kernels.

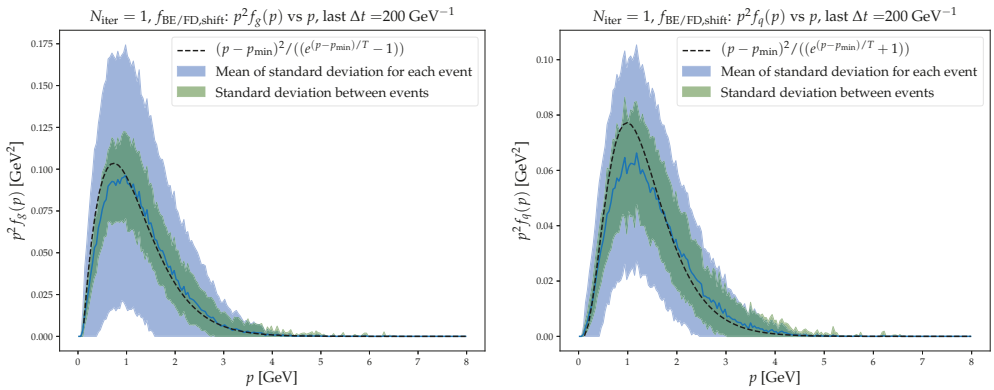

Figure 16: Distribution of the system extracted after the run is finished, averaged over the last $\Delta t = 200$ GeV^{-1}. The blue error bands correspond to mean of the fluctuations within each event over time, while the green error bands correspond to the standard deviation between events. All details about the figures can be found in Paper II. Left: $f_g(p)$. Right: $f_q(p)$.

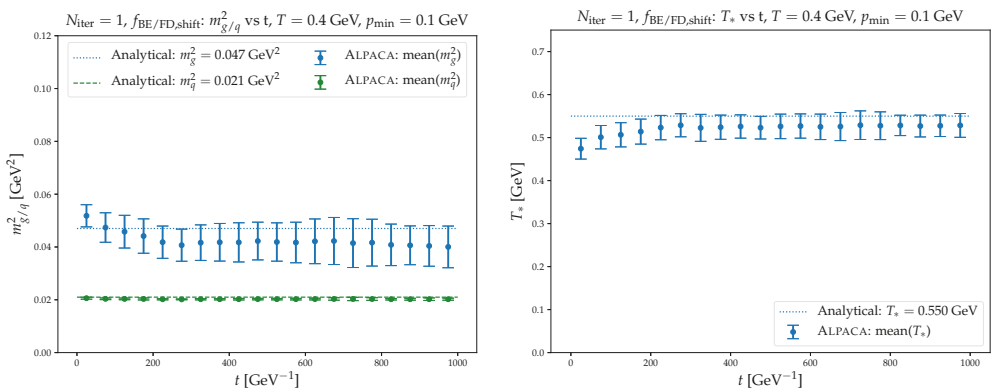

Figure 17: Left: effective mass $m^2_{g/q}$ plotted as a function of time in the long run. Right: Effective temperature T_* as a function of time in the long run. All values converge to the expected analytical results (within errors). All details about the figures can be found in Paper II.

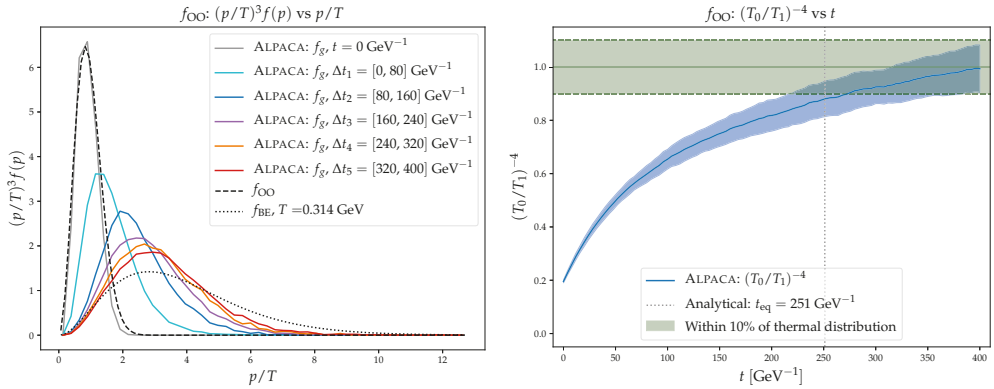

Figure 18: Left: The evolution of the weighted phase space density, $(p/T)^3 f(p)$ as a function of p/T. The dashed line indicates the initial distribution which is sampled from, and the dotted line is the Bose-Einstein distribution with corresponding effective temperature. Solid lines indicate the sampled weighted distribution at different times in ALPACA. Right: time evolution of the ratio of effective temperatures. When reaching $(T_0/T_1)^{-4} = 0.9$ the system is defined as being thermalized. The dotted line indicates the known analytical equilibration time. All details about the figures can be found in Paper III.

5.5 Thermalization

Thermalization is, simply put, when a system starts with a phase space distribution which is out-of-equilibrium and then evolves to equilibrium. Having validated our model starting out from equilibrium, we also want to look at how it can smoothly get to such a configuration. This is a well studied problem in kinetic theory, see e.g. Refs. [55, 60, 61], since it is a central question in heavy ion collisions. As explained in Section 2.2, for a heavy ion collision our system starts out in a highly anisotropic state and then evolve into a QGP which is well described by hydrodynamics. Hence, thermalization (and hydrodynamization) must occur between the pre-equilibrium and equilibrium stage.

In Paper III we look at thermalization in ALPACA. We initialize our system in an overoccupied state, i.e. with an excess of low-momentum gluons, and analyse how the system relaxes into a thermal equilibrium. We find that the system does relax to the correct distribution, in the correct time compared to known analytical results, see Fig. 18. We also look at anisotropic initial conditions, with the momentum in the z-direction being smaller on average than that in the transverse direction. Also here we observe that the system relaxes into a thermal equilibrium with the same longitudinal and transverse pressure.

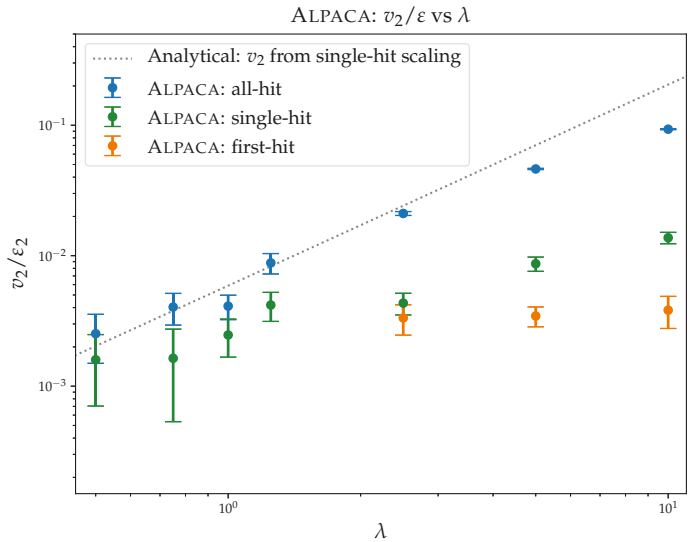

Figure 19: Elliptic flow v_2 over initial eccentricity, as a function of the coupling λ. The results are extracted from ALPACA using the CGC-like initial conditions of Paper I. The dotted line corresponds to the predicted v_2 from the scaling formula derived in Paper I. All details about the figures can be found in Paper IV.

5.6 Small collision systems and single-hit

Lastly, in Paper IV, we look at the CGC-like initial conditions used in Paper I, in ALPACA, and compare our results to those of Paper I. This leads to a number of interesting observations. First, we find that the average number of scatterings per particle in ALPACA is much larger than one for the parameter points we test from Paper I. We then discuss how to reduce the number of scatterings in ALPACA to get a valid comparison to the single hit model. We look at the differences between first-hit, which is letting each parton scatter at most one time, and single-hit, which we implement by rejecting scatterings in the system in a way so that the average number of scatterings per particle is one. We then move on to find that the cross sections in ALPACA are very large for the parameter points of Paper I, and so the elastic scatterings are not local in space. Since the argument of the escape mechanism relies on local isotropization, and our scatterings are (on average) non-local, it becomes less applicable, and we expect a reduction in the produced v_2. We find that this is indeed the case, as shown in Fig. 19.

6 Conclusions and outlook

Recent observations of collective behaviour like signals in $\mathrm{p}+\mathrm{p}$ collisions highlight a clear contradiction in our traditional view of small collision systems lacking final state interac-

tions. The lack of observed jet quenching in the same type of system further complicates the question, as we cannot simply assume that a hydrodynamic QGP will work as a starting point to solve the problem. In this thesis, I, along with my collaborators work towards resolving this contradiction. We do this by looking at different ways in which the QCD effective kinetic theory of AMY can explain the transport of partons from the initial state up until hadronization, while producing collective flow along the way. For large enough systems it should also thermalize over time into a fluid which is well described by hydrodynamics.

We approach this in two ways, the first being more analytical by assuming that partons are only allowed to scatter once. With this simplifying assumption we can extract an analytical expression of the collective flow from AMY, and look at its different scaling properties. The second, and main, approach of this thesis is by constructing the event generator Alpaca, which encodes the dynamics of AMY to evolve particle ensembles in a Lorentz invariant way.

In this introduction I started by giving an overview of the theory needed to explain the contradiction revealed by the measurement of collective behaviour like signals in small systems. I then show the numerical methods needed to extract relevant information from theory; Monte Carlo methods. I then moved on to give an overview of the theory which could act to resolve the contradiction, the QCD effective kinetic theory of AMY. This was followed by an overview of Alpaca. I now end this thesis by summarizing each paper as well as outline possible future work for each paper.

In we employ the single-hit method to study collective flow response to initial geometry deformations of CGC-like initial conditions, in AMY kinetic theory. We derive a scaling formula for the energy flow coefficients following the conformal scaling of the Boltzmann equations, and numerically extract the non-trivial parts which cannot be scaled out analytically, resulting a in pocket formula for elliptic flow. We also show how flow is produced as described in the escape mechanism, and compare the results to the Isotropization Time Approximation. Lastly, we look at the predicted elliptic flow from this method with initial parameters corresponding to small collision systems. The next step in developing this model would be to go beyond the single-hit linearization and allow for multiple scatterings. Extending the system to include quarks would also be of interest. To go beyond energy flow at look at particle number flow would also be of interest, which would require the splitting and merging collision kernel to be included.

In Paper II we introduce Alpaca, and show the details of all the parts of the implementation of AMY kinetic theory as an event generator. We also show the validation in thermal equilibrium, both piecewise for the different dynamics, as well as for the case of all the parts of the implementation active at the same time.

In Paper III we employ the newly validated Alpaca to look at how different systems thermalize and isotropize. We start by looking at under and over-occupied thermal equilibrium to see at which rate it thermalizes, and how this and the evolution of the phase space density to thermal equilibrium compares to known analytical results. We also look at homogeneous anisotropic Color Glass Condensate-like initial conditions, similar to those in Paper I but with no spatial perturbation, to analyse the isotropization processes. By looking at the

evolution of the longitudinal and transverse pressure we find that the system isotropizes as expected, though we have no known analytical results to compare the isotropization time to.

In Paper IV we look at how Alpaca compares to the single-hit model studied in Paper I. We use the same anisotropic, non-homogeneous Color Glass Condensate-like initial conditions and first run simulations with no restrictions on the number of scatterings. We find that Alpaca has a number of scatterings per particle which is on average much larger than one for the parameter points of Paper I we compare to. We also discuss the differences between first-hit and single-hit, where in the former particles are restricted to scatter at most once, and in the latter where the average number of scatterings per particle is one. We also note that elastic scatterings in Alpaca happen in a very non-local way for large values of the coupling, which produces quantitative differences in the extracted collective flow.

In terms of the validation in thermal equilibrium there is nothing more to do, since we consider the implementation validated in this case. Apart from the general development of Alpaca, there are numerous other interesting applications which can be studied currently. Looking at how to extract transport coefficients like shear and bulk viscosity from Alpaca would be of interest. The equilibration processes also requires further study, looking at both thermalization for under-occupied initial conditions, as well as isotropization in a setup for which there exists analytical results to compare to.

As for the general development of Alpaca, there is much to be done. The aim is for Alpaca to be a complete Monte Carlo event generator, hence, proper initial conditions corresponding to small and large collisions would be the next step. There also needs to be a hadronization model, as well as a transport model for hadrons which allow for hadronic re-scattering.

Bibliography

[1] P. B. Arnold, G. D. Moore, and L. G. Yaffe, "Effective kinetic theory for high temperature gauge theories," JHEP **01** (2003) 030, arXiv:hep-ph/0209353 [hep-ph].

[2] T. Nagel, The view from nowhere. Oxford University Press, 1989.

[3] **ATLAS** Collaboration, G. Aad et al., "Observation of a new particle in the search for the Standard Model Higgs boson with the ATLAS detector at the LHC," Phys. Lett. B **716** (2012) 1–29, arXiv:1207.7214 [hep-ex].

[4] **CMS** Collaboration, S. Chatrchyan et al., "Observation of a New Boson at a Mass of 125 GeV with the CMS Experiment at the LHC," Phys. Lett. B **716** (2012) 30–61, arXiv:1207.7235 [hep-ex].

[5] X. Fan, T. G. Myers, B. A. D. Sukra, and G. Gabrielse, "Measurement of the Electron Magnetic Moment," Phys. Rev. Lett. **130** no. 7, (2023) 071801, arXiv:2209.13084 [physics.atom-ph].

[6] **Super-Kamiokande** Collaboration, Y. Fukuda et al., "Evidence for oscillation of atmospheric neutrinos," Phys. Rev. Lett. **81** (1998) 1562–1567, arXiv:hep-ex/9807003.

[7] **SNO** Collaboration, Q. R. Ahmad et al., "Direct evidence for neutrino flavor transformation from neutral current interactions in the Sudbury Neutrino Observatory," Phys. Rev. Lett. **89** (2002) 011301, arXiv:nucl-ex/0204008.

[8] M. E. Peskin and D. V. Schroeder, An Introduction to quantum field theory. Addison-Wesley, Reading, USA, 1995.

[9] **Particle Data Group** Collaboration, R. L. Workman and Others, "Review of Particle Physics," PTEP **2022** (2022) 083C01.

[10] **PHENIX** Collaboration, K. Adcox et al., "Formation of dense partonic matter in relativistic nucleus-nucleus collisions at RHIC: Experimental evaluation by the PHENIX collaboration," Nucl. Phys. A **757** (2005) 184–283, arXiv:nucl-ex/0410003.

[11] **STAR** Collaboration, J. Adams et al., "Experimental and theoretical challenges in the search for the quark gluon plasma: The STAR Collaboration's critical assessment of the evidence from RHIC collisions," Nucl. Phys. A **757** (2005) 102–183, arXiv:nucl-ex/0501009.

[12] **PHOBOS** Collaboration, B. B. Back et al., "The PHOBOS perspective on discoveries at RHIC," Nucl. Phys. A **757** (2005) 28–101, arXiv:nucl-ex/0410022.

[13] **BRAHMS** Collaboration, I. Arsene et al., "Quark gluon plasma and color glass condensate at RHIC? The Perspective from the BRAHMS experiment," Nucl. Phys. A **757** (2005) 1–27, arXiv:nucl-ex/0410020.

[14] H. Satz, "The Quark-Gluon Plasma: A Short Introduction," Nucl. Phys. A **862-863** (2011) 4–12, arXiv:1101.3937 [hep-ph].

[15] R. Pasechnik and M. Šumbera, "Phenomenological Review on Quark–Gluon Plasma: Concepts vs. Observations," Universe **3** no. 1, (2017) 7, arXiv:1611.01533 [hep-ph].

[16] J. C. Collins and M. J. Perry, "Superdense Matter: Neutrons Or Asymptotically Free Quarks?," Phys. Rev. Lett. **34** (1975) 1353.

[17] N. Cabibbo and G. Parisi, "Exponential Hadronic Spectrum and Quark Liberation," Phys. Lett. B **59** (1975) 67–69.

[18] D. T. Son and A. O. Starinets, "Viscosity, Black Holes, and Quantum Field Theory," Ann. Rev. Nucl. Part. Sci. **57** (2007) 95–118, arXiv:0704.0240 [hep-th].

[19] P. Kovtun, D. T. Son, and A. O. Starinets, "Viscosity in strongly interacting quantum field theories from black hole physics," Phys. Rev. Lett. **94** (2005) 111601, arXiv:hep-th/0405231.

[20] B. Muller, J. Schukraft, and B. Wyslouch, "First Results from Pb+Pb collisions at the LHC," Ann. Rev. Nucl. Part. Sci. **62** (2012) 361–386, arXiv:1202.3233 [hep-ex].

[21] **ALICE** Collaboration, J. Adam et al., "Direct photon production in Pb-Pb collisions at $\sqrt{s_{NN}} = 2.76$ TeV," Phys. Lett. B **754** (2016) 235–248, arXiv:1509.07324 [nucl-ex].

[22] M. J. Fromerth, I. Kuznetsova, L. Labun, J. Letessier, and J. Rafelski, "From Quark-Gluon Universe to Neutrino Decoupling: 200 < T < 2MeV," Acta Phys. Polon. B **43** no. 12, (2012) 2261–2284, arXiv:1211.4297 [nucl-th].

[23] W. Busza, K. Rajagopal, and W. van der Schee, "Heavy Ion Collisions: The Big Picture, and the Big Questions," Ann. Rev. Nucl. Part. Sci. **68** (2018) 339–376, arXiv:1802.04801 [hep-ph].

[24] S. Voloshin and Y. Zhang, "Flow study in relativistic nuclear collisions by Fourier expansion of Azimuthal particle distributions," Z. Phys. C **70** (1996) 665–672, arXiv:hep-ph/9407282.

[25] A. M. Poskanzer and S. A. Voloshin, "Methods for analyzing anisotropic flow in relativistic nuclear collisions," Phys. Rev. C **58** (1998) 1671–1678, arXiv:nucl-ex/9805001.

[26] R. Snellings, "Collective Expansion at the LHC: selected ALICE anisotropic flow measurements," J. Phys. G **41** no. 12, (2014) 124007, arXiv:1408.2532 [nucl-ex].

[27] **CMS** Collaboration, "CMS collision events: from lead ion collisions," 2010. CMS Collection.

[28] **ALICE** Collaboration, J. Adam et al., "Enhanced production of multi-strange hadrons in high-multiplicity proton-proton collisions," Nature Phys. **13** (2017) 535–539, arXiv:1606.07424 [nucl-ex].

[29] Z. Citron et al., "Report from Working Group 5: Future physics opportunities for high-density QCD at the LHC with heavy-ion and proton beams," CERN Yellow Rep. Monogr. 7 (2019) 1159–1410, arXiv:1812.06772 [hep-ph].

[30] **CMS** Collaboration, V. Khachatryan et al., "Observation of Long-Range Near-Side Angular Correlations in Proton-Proton Collisions at the LHC," JHEP **09** (2010) 091, arXiv:1009.4122 [hep-ex].

[31] **CMS** Collaboration, S. Chatrchyan et al., "Multiplicity and Transverse Momentum Dependence of Two- and Four-Particle Correlations in pPb and PbPb Collisions," Phys. Lett. B **724** (2013) 213–240, arXiv:1305.0609 [nucl-ex].

[32] **ALICE** Collaboration, S. Acharya et al., "Investigations of Anisotropic Flow Using Multiparticle Azimuthal Correlations in pp, p-Pb, Xe-Xe, and Pb-Pb Collisions at the LHC," Phys. Rev. Lett. **123** no. 14, (2019) 142301, arXiv:1903.01790 [nucl-ex].

[33] **PHENIX** Collaboration, S. S. Adler et al., "Absence of suppression in particle production at large transverse momentum in S(NN)**(1/2) = 200-GeV d + Au collisions," Phys. Rev. Lett. **91** (2003) 072303, arXiv:nucl-ex/0306021.

[34] **STAR** Collaboration, J. Adams et al., "Evidence from d + Au measurements for final state suppression of high p(T) hadrons in Au+Au collisions at RHIC," Phys. Rev. Lett. **91** (2003) 072304, arXiv:nucl-ex/0306024.

[35] **BRAHMS** Collaboration, I. Arsene et al., "Transverse momentum spectra in Au+Au and d+Au collisions at s**(1/2) = 200-GeV and the pseudorapidity dependence of high p(T) suppression," Phys. Rev. Lett. **91** (2003) 072305, arXiv:nucl-ex/0307003.

[36] **CMS** Collaboration, V. Khachatryan et al., "Charged-particle nuclear modification factors in PbPb and pPb collisions at $\sqrt{s_{\mathrm{N\,N}}} = 5.02$ TeV," JHEP **04** (2017) 039, arXiv:1611.01664 [nucl-ex].

[37] J. Brewer, A. Mazeliauskas, and W. van der Schee, "Opportunities of OO and pO collisions at the LHC," in Opportunities of OO and pO collisions at the LHC. 3, 2021. arXiv:2103.01939 [hep-ph].

[38] C. Bierlich, G. Gustafson, and L. Lönnblad, "Collectivity without plasma in hadronic collisions," Phys. Lett. B **779** (2018) 58–63, arXiv:1710.09725 [hep-ph].

[39] C. Bierlich, S. Chakraborty, G. Gustafson, and L. Lönnblad, "Setting the string shoving picture in a new frame," JHEP **03** (2021) 270, arXiv:2010.07595 [hep-ph].

[40] C. Bierlich et al., "A comprehensive guide to the physics and usage of PYTHIA 8.3" SciPost Phys. Codebases **8** (3, 2022) , arXiv:2203.11601 [hep-ph].

[41] **Sherpa** Collaboration, E. Bothmann et al., "Event Generation with Sherpa 2.2" SciPost Phys. 7 no. 3, (2019) 034, arXiv:1905.09127 [hep-ph].

[42] J. Bellm et al., "Herwig 7.0/Herwig++ 3.0 release note," Eur. Phys. J. C **76** no. 4, (2016) 196, arXiv:1512.01178 [hep-ph].

[43] M. Bahr et al., "Herwig++ Physics and Manual," Eur. Phys. J. C **58** (2008) 639–707, arXiv:0803.0883 [hep-ph].

[44] K. C. Zapp, "JEWEL 2.0.0: directions for use," Eur. Phys. J. C **74** no. 2, (2014) 2762, arXiv:1311.0048 [hep-ph].

[45] Z.-W. Lin, C. M. Ko, B.-A. Li, B. Zhang, and S. Pal, "A Multi-phase transport model for relativistic heavy ion collisions," Phys. Rev. C **72** (2005) 064901, arXiv:nucl-th/0411110.

[46] Z.-W. Lin and L. Zheng, "Further developments of a multi-phase transport model for relativistic nuclear collisions," Nucl. Sci. Tech. **32** no. 10, (2021) 113, arXiv:2110.02989 [nucl-th].

[47] X.-N. Wang and M. Gyulassy, "HIJING: A Monte Carlo model for multiple jet production in p p, p A and A A collisions," Phys. Rev. D **44** (1991) 3501–3516.

[48] H. Van Hees, "Introduction to relativistic transport theory," https://itp.uni-frankfurt.de/~hees/publ/kolkata.pdf, 2022. Visited on 2023-08-28.

[49] B. L. Combridge, J. Kripfganz, and J. Ranft, "Hadron Production at Large Transverse Momentum and QCD," Phys. Lett. B **70** (1977) 234.

[50] R. A. Treumann, R. Nakamura, and W. Baumjohann, "Relativistic transformation of phase-space distributions," Ann. Geophys. **29** (2011) 1259–1265, arXiv:1105.2120 [physics.space-ph].

[51] M. C. Abraao York, A. Kurkela, E. Lu, and G. D. Moore, "UV cascade in classical Yang-Mills theory via kinetic theory," Phys. Rev. D **89** no. 7, (2014) 074036, arXiv:1401.3751 [hep-ph].

[52] J. Ghiglieri, G. D. Moore, and D. Teaney, "Jet-Medium Interactions at NLO in a Weakly-Coupled Quark-Gluon Plasma," JHEP **03** (2016) 095, arXiv:1509.07773 [hep-ph].

[53] A. Kurkela and A. Mazeliauskas, "Chemical equilibration in weakly coupled QCD," Phys. Rev. D **99** no. 5, (2019) 054018, arXiv:1811.03068 [hep-ph].

[54] A. Kurkela, U. A. Wiedemann, and B. Wu, "Opacity dependence of elliptic flow in kinetic theory," Eur. Phys. J. C **79** no. 9, (2019) 759, arXiv:1805.04081 [hep-ph].

[55] A. Kurkela and Y. Zhu, "Isotropization and hydrodynamization in weakly coupled heavy-ion collisions," Phys. Rev. Lett. **115** no. 18, (2015) 182301, arXiv:1506.06647 [hep-ph].

[56] T. Lappi, "Gluon spectrum in the glasma from JIMWLK evolution," Phys. Lett. **B703** (2011) 325–330, arXiv:1105.5511 [hep-ph].

[57] D. Currie, T. Jordan, and E. Sudarshan, "Relativistic invariance and Hamiltonian theories of interacting particles," Rev.Mod.Phys. **35** (1963) 350–375.

[58] G. Peter, D. Behrens, and C. C. Noack, "Poincare covariant particle dynamics. 1: Intranuclear cascade model," Phys. Rev. C **49** (1994) 3253–3265.

[59] V. Borchers, J. Meyer, S. Gieseke, G. Martens, and C. C. Noack, "A Poincare covariant parton cascade model for ultrarelativistic heavy ion reactions," Phys. Rev. C **62** (2000) 064903, arXiv:hep-ph/0006038.

[60] Y. Fu, J. Ghiglieri, S. Iqbal, and A. Kurkela, "Thermalization of non-Abelian gauge theories at next-to-leading order," Phys. Rev. D **105** no. 5, (2022) 054031, arXiv:2110.01540 [hep-ph].

[61] A. Kurkela and E. Lu, "Approach to Equilibrium in Weakly Coupled Non-Abelian Plasmas," Phys. Rev. Lett. **113** no. 18, (2014) 182301, arXiv:1405.6318 [hep-ph].

Overview of publications

In this section I briefly summarise the content of each paper, as well as specify what have been my individual contributions. In the field of theoretical particle physics, all authors are listed alphabetically.

Paper I

Collective flow in single-hit QCD kinetic theory

Aleksi Kurkela, Aleksas Mazeliauskas, **Robin Törnkvist**
JHEP **11** 216 (2021)
e-print: `arXiv:2104.08179 [hep-th]`

We derive results from the single-hit approximation of AMY kinetic theory looking specifically of the energy flow response to initial geometrical deformations in a purely gluonic system.

The work was based on the ideas of Aleksi Kurkela, and the numerical implementation was done mainly by me, with support and guidance from Aleksas Mazeliauskas, using code that Aleksi and Aleksas had created as the underlying framework of the new code. Implementations of a phase-space sampler and matrix elements was also used from the already existing code. Calculations of the analytical expression for the collective flow coefficients as well as the scaling formulas were done in collaboration.

In the article I wrote Appendix A and B, as well as large parts of Section 2. I also contributed to parts of section 3. All plots and illustrations, as well as all numerical results have been created by me, except the one in Section 3.3.

Paper II

AMY Lorentz invariant parton cascade - the thermal equilibrium case

Aleksi Kurkela, **Robin Törnkvist**, Korinna Zapp
Submitted to Eur.Phys.J.C
e-print: `arXiv:2211.15454 [hep-ph]`

In this paper we introduce the Lorentz invariant parton cascade Alpaca. We show the details of how it is implemented to faithfully reproduce the dynamics of AMY kinetic theory, and verify it in the case of an infinite thermal equilibrium.

The work was based on the ideas of Korinna Zapp, and started out based on a proof-of-concept code which she had implemented. The original code contained the Lorentz invariant evolution scheme as well as elastic scattering with a constant infra-red regulator. Turning this into a faithful representation of the AMY effective kinetic theory required

extensive further developments of codes, most notably the dynamic extraction of the effective masses and temperature, and implementation of splitting and merging processes. I was heavily involved in the development of the algorithms and did all of the implementation and code validation, except for the solution to the periodic boundary conditions shown in Appendix A, which was developed and implemented by Korinna Zapp. I produced all results and plots shown in the paper, wrote most of Section 4 and Appendix C and contributed to all other sections.

Paper III

Thermalization and isotropization in the AMY parton cascade Alpaca

Robin Törnkvist, Korinna Zapp
To be submitted to Eur.Phys.J.C
e-print: `arXiv:2309.04413 [hep-ph]`

In this article we look at how different systems thermalize and isotropize in the newly developed framework of Alpaca. We analyse two different scenarios; an overoccupied thermal system for thermalization, and isoptropization for anisoptropic Color Glass Condensate-like initial conditions. We find that the system thermalizes in the correct manner with a correct thermalization time (within errors) compared to known analytical and numerical results, for the overoccupied case. For the isotropization we see the correct behaviour in terms of the ratio of longitudinal and transverse pressure evolving to unity.

The code used to extract data is that of Alpaca, which is the code that I have developed as described for Paper II. The primary work of the article, which mainly involved producing additional code for Alpaca as well as extracting and analysing data from the overoccupied and anisoptropic events, was mainly done by me, with guiding help from Korinna Zapp.

For the article I was the main author of all sections. All plots and data shown in the article were produced by me.

Paper IV

Small systems and the single-hit approximation in the AMY parton cascade Alpaca

Robin Törnkvist, Korinna Zapp
Submitted to Phys.Lett.B
e-print: `arXiv:2309.04458 [hep-ph]`

In this article we study small collision systems in Alpaca using Color Glass Condensate-like initial conditions, looking mainly at elliptic collective flow. We compare and discuss the differences of the first-hit, single-hit and all-hit models, i.e. when particles are allowed to scatter once, when the average number of scatterings per particle is one, and when there

are no restrictions on the number of scatterings. We compare our results to those found in Paper I, and find quantitative differences in the extracted collective flow, which depend on generic differences in how the flow is extracted.

The code used to run a majority of the simulations is that of Alpaca, which I have developed as described for Paper II. I did most of the work related to Alpaca in this project, with guidance from Korinna Zapp. This mainly involved implementing the modifications needed for Alpaca to be able to run the relevant analyses for this project, as well as well as extracting and analysing relevant data.

The article was written in collaboration, where I was the main author of Section 5 and contributed to large parts of Section 4. All figures and data related to Alpaca were produced by me.